

PRODUCTION OF NANOFIBERS BY ELECTROSPINNING FOR
INTERFACIAL TOUGHENING OF COMPOSITES

A THESIS SUBMITTED TO
THE GRADUATE SCHOOL OF NATURAL AND APPLIED SCIENCES
OF
MIDDLE EAST TECHNICAL UNIVERSITY

BY

ZEYNEP CANSU ÖZÇINAR

IN PARTIAL FULFILLMENT OF THE REQUIREMENTS
FOR
THE DEGREE OF MASTER OF SCIENCE
IN
CHEMICAL ENGINEERING

SEPTEMBER 2019

Approval of the thesis:

**PRODUCTION OF NANOFIBERS BY ELECTROSPINNING FOR
INTERFACIAL TOUGHENING OF COMPOSITES**

submitted by **ZEYNEP CANSU ÖZÇINAR** in partial fulfillment of the requirements
for the degree of **Master of Science in Chemical Engineering Department, Middle
East Technical University** by,

Prof. Dr. Halil Kalıpçılar
Dean, Graduate School of **Natural and Applied Sciences**

Prof. Dr. Pınar Çalık
Head of Department, **Chemical Engineering**

Assoc. Prof. Dr. Erhan Bat
Supervisor, **Chemical Engineering, METU**

Prof. Dr. Bora Maviş
Co-Supervisor, **Mechanical Eng., Hacettepe Uni.**

Examining Committee Members:

Prof. Dr. Cevdet Kaynak
Metallurgical and Materials Engineering, METU

Assoc. Prof. Dr. Erhan Bat
Chemical Engineering, METU

Prof. Dr. Bora Maviş
Mechanical Engineering, Hacettepe Uni.

Assoc. Prof. Dr. İrem Erel Göktepe
Chemistry, METU

Assist. Prof. Dr. Emre Büküşoğlu
Chemical Engineering, METU

Date: 02.09.2019

I hereby declare that all information in this document has been obtained and presented in accordance with academic rules and ethical conduct. I also declare that, as required by these rules and conduct, I have fully cited and referenced all material and results that are not original to this work.

Name, Surname: Zeynep Cansu Özçınar

Signature:

ABSTRACT

PRODUCTION OF NANOFIBERS BY ELECTROSPINNING FOR INTERFACIAL TOUGHENING OF COMPOSITES

Özçınar, Zeynep Cansu
Master of Science, Chemical Engineering
Supervisor: Assoc. Prof. Dr. Erhan Bat
Co-Supervisor: Prof. Dr. Bora Maviş

September 2019, 104 pages

In this work, electrospinning technique was selected for the production of nanofiber mats to be used in improving the fracture toughness of carbon fiber reinforced composites. The main purpose of this study is to improve G_{IC} delamination mode of polyamide-6 (PA6) nanofibers interleaved carbon fiber reinforced polymer (CFRP) composite. Many studies [1]-[4] have shown that when PA6 nanofiber is used as an interleaving material for improving delamination modes of composites G_{IIC} sliding mode could be significantly increased. However, G_{IC} opening mode could not be improved or even worsened. In an attempt to solve this problem, nanofibers were produced with different combinations and mass ratios of Polyamide 6 (PA6), poly (trimethylene carbonate) (PTMC), poly (ϵ -caprolactone) (PCL) and shellac polymers. These nanofibers were used as an interleaving material for carbon fiber reinforced polymer (CFRP) composites. G_{IC} fracture toughness of produced composite laminates were tested by means of Double Cantilever Beam (DCB) test. After this test, fracture surfaces of composites were analyzed with the help of Scanning Electron Microscopy (SEM). Among the all results obtained during this study, 13% enhancement in G_{IC} initiation stage compared to neat composite laminate were obtained with combination of PA6 nanofiber and shellac beads interleaving mat.

Keywords: Electrospinning, polyamide-6, delamination, shellac, carbon fiber reinforced composites

ÖZ

KOMPOZİT ARAYÜZEYLERİNİ GÜÇLENDİRMEK İÇİN ELEKTRO- EĞİRME YÖNTEMİYLE NANOFİBER ÜRETİMİ

Özçınar, Zeynep Cansu
Yüksek Lisans, Kimya Mühendisliği
Tez Danışmanı: Doç. Dr. Erhan Bat
Ortak Tez Danışmanı: Prof. Dr. Bora Maviş

Eylül 2019, 104 sayfa

Bu çalışmada, karbon fiber takviyeli kompozitlerin ara yüzey tokluklarını arttırmak amacıyla kullanılacak olan nanoliflerin üretimi için elektroegirme yöntemi seçilmiştir. Çalışmanın asıl amacı, poliamid-6 (PA6) nanolif katkılı karbon fiber takviyeli polimer (KFTP) kompozitinin G_{IC} delaminasyon modunu geliştirmektir. Birçok çalışma [1]-[4] göstermiştir ki PA6'nın ara yüzey katkı malzemesi olarak kullanıldığı KFTP kompozitlerinin G_{IIC} kayma modunda önemli bir artış sağlanabilmiştir. Fakat, G_{IC} açılma modunda artış sağlanamamış hatta daha da kötüye gitmiştir. Bu problemi çözebilmek için poliamid-6 (PA6), poli (trimetilen karbonat) (PTMC), polikaprolakton (PCL) ve şellak polimerlerinin farklı kombinasyon ve kütle oranları ile nanofiberler üretilmiştir. Üretilen bu nanofiberler, KFTP kompozitlerinde ara yüzey toklaştırıcı malzeme olarak kullanılmıştır. Üretilen kompozit laminatların G_{IC} kırılma tokluğu, Çift Ankastre Kiriş (DCB) testi ile ölçülmüştür. Bu testten sonra, Taramalı Elektron Mikroskobu (SEM) yardımıyla kırılan kompozitlerin ara yüzleri analiz edilmiştir. Bu çalışma boyunca elde edilen tüm sonuçlar arasında eklentisiz kompozit laminatına kıyasla G_{IC} başlangıç değerinde %13'lük bir artış PA6 nanofiber ve şellak boncuklarının oluşturduğu tül kombinasyonunun kompozit ara yüzeyine eklenmesiyle elde edilmiştir.

Anahtar Kelimeler: Elektroeđirme, Polyamid-6, delaminasyon, řellak, karbon fiber takviyeli kompozit

To my well-beloved family

ACKNOWLEDGEMENTS

First of all, I would like to express my gratitude to my supervisor Erhan Bat and co-supervisor Bora Maviş due to giving a chance to be a part of their teams, and also their patience and valuable suggestions over the last three years. At first Nur Merve Kazarođlu, special thanks to my lab colleagues Gzde Őahin, Cansu aylan, Cemre Avşar, Ayşe Elif Kırathlı and Duygu Sezen Polat for their kindly support in every aspect of my life during this long journey. I wish to special thanks to znur Dođan. I am forever grateful for her valuable advice, endless support and energy. Also, I express my sincere thanks to Elif Manuođlu and Esra Atıcı for their endless friendship, encouragement and keeping me sane throughout my academic life. I am grateful to my managers in B/S/H/, Bora Kayıkçı and Cemalettin Hastrk, for giving a permission to spend time on my study. I would like to give my special appreciation to UNAM and Hacettepe University for allowing me to use their resources during my study. I owe many thanks to my dearie family; Nesim and Hlyya zınar. Whatever I chose, they always support me with their endless love and encouragement throughout my life. My deepest gratitude goes to my lovely aunts, Berna Arslantaş and Selma Toktaş. While I am growing up, their invaluable encouragement made a huge contribution in shaping who and where I am today. Also, I would like to thank my little cousins Bulut and Su Toktaş for coloring my life. The last but not least, I am indebted to Deniz Kayacan for his encouragement, understanding and unfailing support during the hard times.

TABLE OF CONTENTS

ABSTRACT	v
ÖZ	vii
ACKNOWLEDGEMENTS	x
TABLE OF CONTENTS	xi
LIST OF TABLES	xiii
LIST OF FIGURES	xiv
LIST OF ABBREVIATIONS	xviii
LIST OF SYMBOLS	xx
1. INTRODUCTION	1
2. BACKGROUND AND LITERATURE SURVEY	9
2.1. Composite Materials.....	9
2.1.1. Classification of Composite Materials.....	10
2.1.2. Advantages and Disadvantages of Composites	12
2.1.3. Composite Laminates	13
2.1.4. Failure and Damage Mechanisms for Composite Laminates	15
2.2. Delamination	16
2.2.1. Delamination Modes.....	17
2.2.2. Sources of Delamination.....	22
2.2.3. Proposed Solutions to Delamination Failure	23
2.3. Electrospinning.....	33
2.3.1. Parameters for Electrospinning.....	35
2.4. Polymers Used in Nanofiber Production for Interfacial Toughening (IFT)....	37

3. MATERIALS AND METHODS	43
3.1. Materials.....	43
3.2. Methods.....	44
3.2.1. Synthesis of PTMC (Two-armed Low Molecular Weight PTMC).....	44
3.2.2. Preparation of Electrospinning Solutions.....	44
3.2.3. Production of Nanofibers via Electrospinning.....	46
3.2.4. Production of Composite Laminates	51
3.3. Characterizations.....	53
3.3.1. Gel Permeation Chromatography (GPC)	53
3.3.2. Scanning Electron Microscopy (SEM).....	53
3.3.3. Double Cantilever Beam (DCB) Test	53
4. RESULTS AND DISCUSSIONS	55
4.1. PTMC Synthesis	55
4.2. Production of Nanofibers	55
4.3. DCB Test Results.....	63
4.4. Analysis of Fracture Surfaces	69
5. CONCLUSIONS	81
6. RECOMMENDATIONS	85
REFERENCES	87
A. Gel Permeation Chromatogram of Synthesized PTMC	93
B. The Contents of Electrospinning and Electrospaying Solutions.....	94
C. Example for Calculation of G_{IC} According to ASTM-D5528	97

LIST OF TABLES

TABLES

Table 2.1 Composite types,their properties and applications	12
Table 2.2 Pros and cons of composites	13
Table 2.2 Summary for limitation of proposed solution techniques.....	24
Table 2.4 Polymers used in IFT and their effects on G_{IC}	38
Table 3.1 Mechanical properties of prepreg	43
Table 3.2 Solution contents in terms of solvent and polymer type.....	45
Table 3.3 Electrospinning/electrospraying process parameters for each ES	49
Table 4.1 Veils' groups and their aims	56
Table 4.2 Groups and their contents in terms of composite and solution name and polymer used in production.....	64
Table 4.3 DCB test results in terms of GIC initiation and propagation values.....	67
Table 4.4 Percent change in G_{IC} initiation and propagation with respect to Z1 and Z2 laminates	67
Table B 1 Ingredients of electrospinning and electrospraying solutions	94

LIST OF FIGURES

FIGURES

Figure 1.1 Usage of composites in aerospace industry.....	2
Figure 1.2 Types of materials used in the 787.....	3
Figure 1.3 Damages mostly occur in composite laminates	4
Figure 1.4 Chemical structure of shellac.	6
Figure 1.5 Reaction between shellac and epoxy resin.....	6
Figure 2.1 Phases of composites.....	9
Figure 2.2 Classifications of composites based on matrix and reinforcement.	11
Figure 2.3 Carbon fiber prepreg	13
Figure 2.4 Stacking of prepreg plies to a laminate with different angles of fibers....	14
Figure 2.5 Delamination failure mechanism	16
Figure 2.6 Modes of delamination.....	17
Figure 2.7 The geometry of DCB test specimen	18
Figure 2.8 The geometries of Mode II test specimens; (a) ENF; (b) SENF; (c) 4ENF; (d) ELS.....	19
Figure 2.9 The geometries of specimen for Mode III tests; (a) SCB; (b) ECT.	20
Figure 2.10 The geometries of specimen for Mixed-Mode tests; (a) MMB; (b) MMF; (c) CLS; (d) SLFPB; (e) ADCB; (f) the Arcan.....	21
Figure 2.11 Sources of delamination	22
Figure 2.12 The configuration of amine groups, HBPs and epoxy chains	25
Figure 2.13 Constituents used in interleaving	26
Figure 2.14 Representation of cross section of laminate with particles interleaved .	27
Figure 2.15 Relationship between fracture toughness and increment of crack length for T800H/3900-2 particle interleaved laminate and T800H/3631 reference laminate	28
Figure 2.16 Crack path during Mode I measurement	29

Figure 2.17 Representation of laminate cross section with film interleaved	30
Figure 2.18 Relationship between fracture toughness and increment of crack length for UT500/111/Ionomer film interleaved laminates and UT500/111 base laminate .	31
Figure 2.19 Graph of fracture toughness versus crack length of base and interleaved AS4/3501-6 composites	32
Figure 2.20 Schematic of experimental setup for electrospinning.....	34
Figure 2.21 Parameters for electrospinning	35
Figure 2.22 Comparison of G_{IC} and G_{IIC} values for PCL and PA6 nanofibers interleaved composites and reference composite.....	39
Figure 2.23 SEM micrographs of fracture surfaces composites interleaved with PA6 and PCL nanofibers after Mode II loading	40
Figure 2.24 SEM micrographs of fracture surfaces composites interleaved with PA6 and PCL nanofibers after Mode I loading.....	41
Figure 3.1 Chemical structure of two-armed hydroxyl group terminated PTMC.....	44
Figure 3.2 Flow chart for preparation of solutions	45
Figure 3.3 Experimental setup for electrospinning and electrospaying.....	47
Figure 3.4 An oxidized copper plate	47
Figure 3.5 Schematic representation of sandwich structure.....	50
Figure 3.6 Representation of the transferring nanofiber veil to mid-interface of prepregs	51
Figure 3.7 Hot press used for curing composite laminates.	52
Figure 3.8 Temperature profile of curing process.....	52
Figure 3.9 The DCB test specimen.	54
Figure 4.1 Nanofibers SEM micrographs with 10 kX magnification and 10 μ m scale bar.....	58
Figure 4.2 Representation of process for ES-7 and ES-9.....	60
Figure 4.3 SEM micrograph of interleaving mat produced by ES-7	60
Figure 4.4 The SEM micrograph of ES-9 interleaving mat.....	62
Figure 4.5 Representation of process for ES-10	62
Figure 4.6 The SEM micrograph of ES-10 interleaving mat.	63

Figure 4.7 Plot of Group A composites in terms of load and displacement.	65
Figure 4.8 Plot of Group B composites in terms of load and displacement.	65
Figure 4.9 Plot of Group C composites in terms of load and displacement.	66
Figure 4.10 Plot of Group D composites in terms of load and displacement.	66
Figure 4.11 The plot of composites from each group which have greater improvement and reference in terms of G_{IC} and crack length.	68
Figure 4.12 SEM micrograph of fracture surface of PA6 nanointerleaved composite laminate (Z2); (a) initiation, (b) propagation stage.	70
Figure 4.13 SEM micrograph of fracture surface of PA6 and shellac nanointerleaved composite laminate (Z3); (a) initiation, (b) propagation stage.	71
Figure 4.14 SEM micrograph of fracture surface of PA6 and shellac nanointerleaved composite laminate (Z4); (a) initiation, (b) propagation stage.	72
Figure 4.15 SEM micrograph of fracture surface of PA6 and PTMC nanointerleaved composite laminate (Z5); (a) initiation, (b) propagation stage.	73
Figure 4.16 SEM micrograph of fracture surface of PA6, PTMC and shellac nanointerleaved composite laminate (Z6); (a) initiation, (b) propagation stage.	74
Figure 4.17 SEM micrograph of fracture surface of PA6 and shellac nanointerleaved composite laminate (Z7); (a) initiation, (b) propagation stage.	75
Figure 4.18 SEM micrograph of fracture surface of PA6 and shellac nanointerleaved composite laminate (Z8); (a) initiation, (b) propagation stage.	76
Figure 4.19 SEM micrograph of fracture surface of PA6, PCL and shellac nanointerleaved composite laminate (Z9); (a) initiation, (b) propagation stage.	77
Figure 4.20 SEM micrograph of fracture surface of PA6, PCL and shellac nanointerleaved composite laminate (Z10); (a) initiation, (b) propagation stage.	78
Figure 4.21 SEM micrograph of fracture surface of PA6, PCL and shellac nanointerleaved composite laminate (Z11); (a) initiation, (b) propagation stage.	79
Figure A 1 Chromatogram of synthesized two-armed PTMC.	93
Figure C 1. DCB test machine.	97
Figure C 2 Test specimen under loading.	98
Figure C 3 Crack growth along the specimen under loading.	98

Figure C 4 Measured crack length and load values by DCB.	99
Figure C 5 Transfer measured values to Excel in order to calculate fracture toughness.	100
Figure C 6 Correction factor in Modified Beam Theory.	101
Figure C 7 Calculation of Δ	102
Figure C 8 Plot of G_{IC} versus displacement graph with standard deviation.	103
Figure C 9 Plotting graph by using load and displacement data which are measured continuously during the test.	104

LIST OF ABBREVIATIONS

Abbreviations	Definitions
4ENF	Four- point end notched flexure
ADCB	Asymmetric double cantilever beam
ASTM	American Society for Testing and Materials
CFR	Carbon fiber reinforced
CFRP	Carbon fiber reinforced polymer
CLS	Cracked lab shear
CMCs	Ceramic matrix composites
DCB	Double cantilever beam
DMF	N,N-dimethylformamide
ECT	The edge crack torsion
ELS	End loaded split
ENF	End notched flexure
EtOH	Ethanol
GPC	Gel Permeation Chromatography
HBP	Hyper branched polymers
MC	Methylene chloride
MMB	Mixed mode bending
MMCs	Metal matrix composites
MMF	Mixed mode flexure

PA6	Polyamide-6
PCL	Poly (ϵ -caprolactone)
PMCs	Polymer matrix composites
PTMC	Poly (trimethylene carbonate)
PSF	Polysulfones
PVA	Poly (vinyl alcohol)
PVB	Poly (vinyl butyral)
PVDF	Poly (vinylidene fluoride)
SCB	Split cantilever beam
SEM	Scanning electron microscopy
SENF	Stabilized end notched flexure
SH	Shellac
SLFPB	Single leg four point bend
Sn(Oct) ₂	Stannous Octoate
TFE	2,2,2-trifluoroethanol
TMC	Trimethylene carbonate
UNAM	National Nanotechnology Research Center

LIST OF SYMBOLS

Symbols	Definitions
(w/w%)	Weight by weight percent
G_{IC}	Interlaminar fracture toughness
G_{IIC}	Sliding shear fracture toughness
G_{IIIC}	Tearing shear fracture toughness
M_w	Number average molecular weight
T_g	Glass transition temperature
$V_{solution}$	Flow rate
$\rho_{solvent}$	Density

CHAPTER 1

INTRODUCTION

Nowadays, for the aerospace industry, designers are finding a new tool in order to eliminate the obstacles caused by metallic components. In this regard, advanced composite materials are the new black due to their excellent features like lightweight, excellent strength and stiffness compared to other materials. The first use of composite materials dates back to the 1950s for the aerospace industry. In the first place, composites were used in tertiary parts of aircraft such as sidewalls, galleys and bag racks parts of aircraft. They were tried in these interior parts of aircraft since if there was a fail in the structure, this did not cause a harm for flying properties of aircraft. After this attempt was succeed, composites were started to use in secondary parts of aircraft like rudders, flaps, ailerons and so on. Fiberglass was mostly used in these composites [1]. Fiberglass is composed of fine fibers as a reinforcement and plastic as a matrix. It has good mechanical properties like lightweight, strong and durable material [2]. However, in the 1970s, instead of fiberglass, carbon fibers have been started to use in the most of secondary structures because carbon fiber has better properties such as stiffness. For the last twenty years, composite materials have been used in primary structures, i.e. wings, fuselage barrels and stabilizers which are the most critical parts of aircrafts in terms of safety [1]. Figure 1.1 illustrates the enhancement of the usage of carbon fiber reinforced (CFR) composites in military and commercial aircrafts.

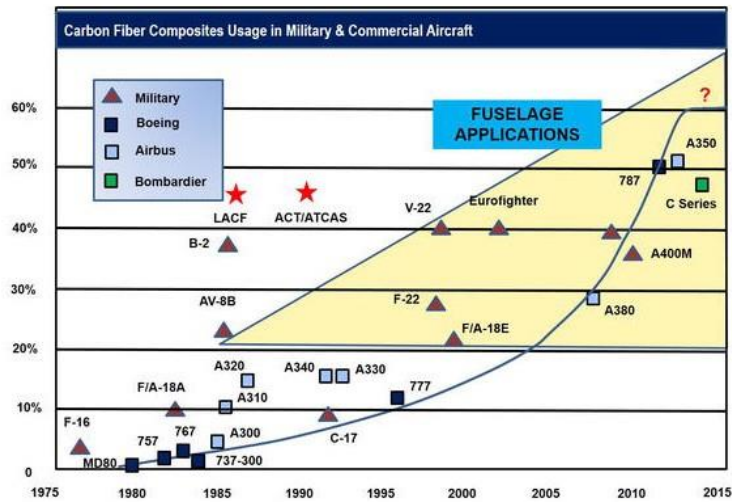


Figure 1.1 Usage of composites in aerospace industry. [1]

For instance, Dreamliner (the 787) is the new generation commercial aircraft whose primary parts were made up of mostly high-performance CFR composites. These primary parts are half of the aircraft and therefore affect total weight since usage of composite materials reduces its total weight correspondingly its performance. Type of materials used in the 787 are shown in Figure 1.2.

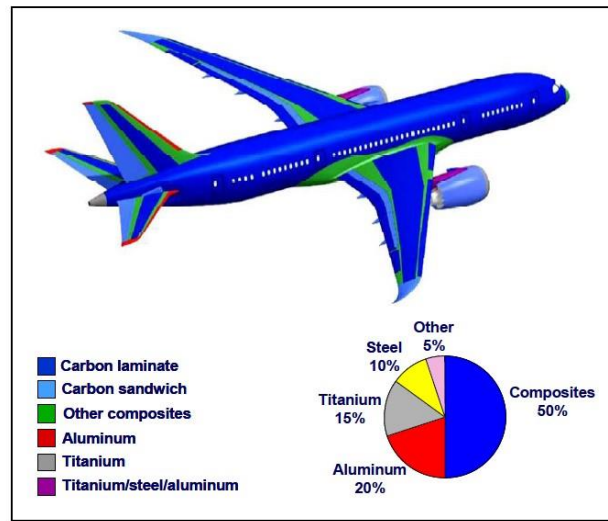


Figure 1.2 Types of materials used in the 787. [1]

According to Figure 1.2, carbon laminate composites are mainly preferred since designers have a chance to find optimum mechanical properties thanks to the laminated structure of these materials. For safe design and endurance of the material, it is important to know failure mechanism and fatigue behavior of composites. They have very complicated failure mechanisms compared to that of metals. Figure 1.3 shows failures which are generally seen in composite laminates.

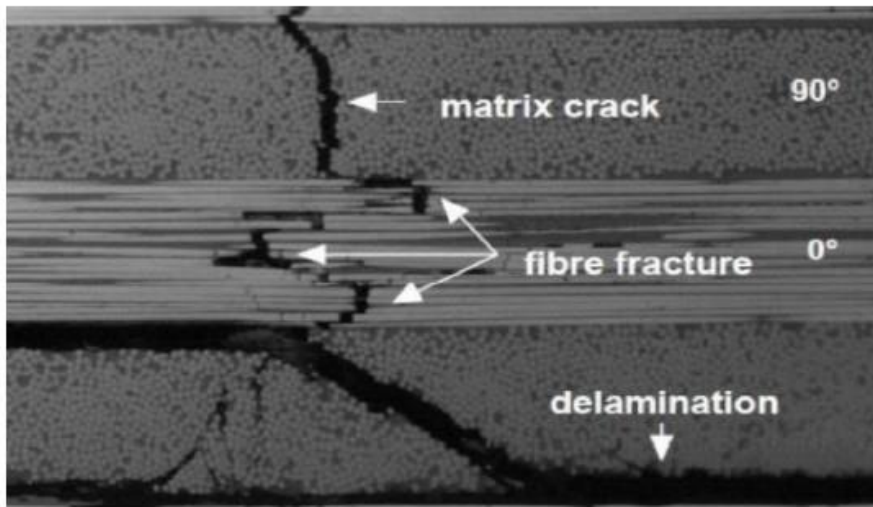


Figure 1.3 Damages mostly occur in composite laminates. [4]

Matrix crack and fiber fracture are the intralaminar damages. These types of damages occur inside the plies. On the other hand, delamination which is the separation of the plies, is the interlaminar damage because it occurs at the interface of two sequential layer [4]. Among them, delamination plays a key role for the design of new structures since it leads to precarious crack growth and directly affects loading capacity of material.

Over the past few decades, many studies have been performed on the healing of delamination failure of the composite laminates. Up to now, various approaches have been attempted in this regard such as matrix toughening, optimization of stacking sequences, edge cap reinforcement, thorough-thickness stitching and ductile interleaving.

In this study, ductile interleaving method has been carried out to develop delamination resistance of the laminate composites. Nanofibers were chosen as interleaving tool. For production of nanofibers, polymers with higher melting temperatures should be used in order to allow a wide range of curing temperatures. PA nanofibers have a great potential since they have typical melting temperatures above 200°C. Also, they are

commonly used for such studies. There are many researches dedicated to the effect of polyamides on delamination of composite laminates. Saghafi [5] and Beckermann [6] stated that G_{IC} and G_{IIC} are enhanced by means of polyamide nanofibers interleaving. Whereas, enhancement in G_{IC} is occurred along pre-crack or crack initiation steps. Propagation value of G_{IC} is not changed or sometimes reduced due to interleaving. In another study, Palazetti [7], [8] et al. reported that only minor improvements and even decreases on both G_{IC} and G_{IIC} . Moreover, according to the study of Schoenmaker [9], Mode I tests proved that there is a small enhancement in the toughness when PA6 nanofibers were interleaved in the glass fiber composite. In there, the thickness of nanofiber veil plays a crucial role. When compared all these findings, PA nanofibers interleaving is worth worked on.

In this study, PA6 is chosen as main polymer because it has great material features such as affordable price, low friction coefficient, high Young's modulus, good stiffness and strength, high wear and chemical resistance [10]. Also, it is compatible with many different polymers. In order to enhance G_{IC} fracture toughness of both neat laminate, and PA6 interleaved laminate composite, shellac, PTMC and PCL are used as assistant polymer in nanofiber production. In this way, adhesion strength and compatibility between matrix and nanofibers have been expected to increase.

The aim of choosing shellac was to achieve good adhesion between matrix and as-spun nanofibers. For that reason, shellac nanoparticles were produced because functional groups in shellac nanoparticles could make covalent bond with the matrix (epoxy resin). Shellac is a natural and non-toxic polymer. Molecular structure of shellac is shown in Figure 1.4 . It consists of hydroxyl group (-OH), carboxyl group (-COOH), ester bond (-COO-), double bond (C=C) and aldehyde group (-CHO).

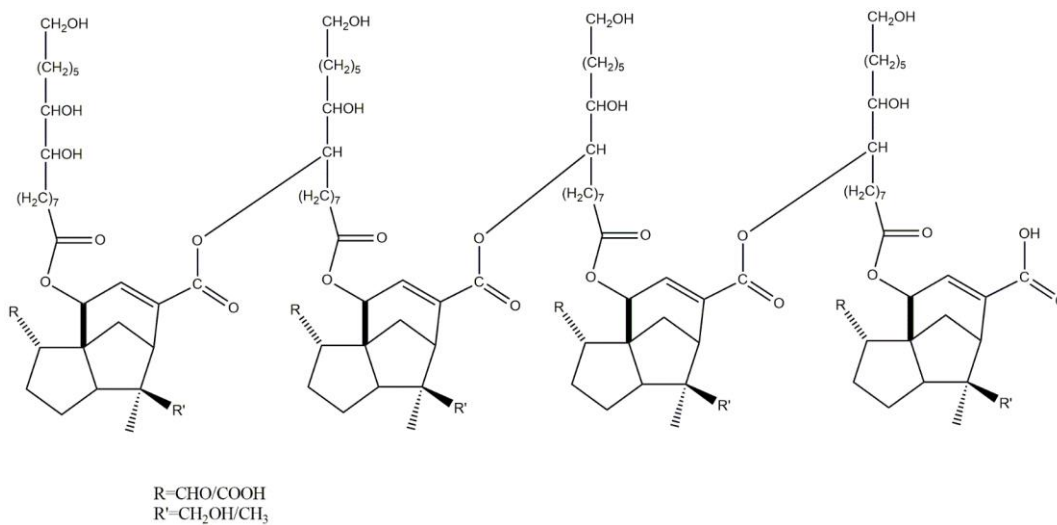


Figure 1.4 Chemical structure of shellac.

Our expectation from shellac polymer is that hydroxyl (-OH) and carboxyl groups (-COOH) of shellac react with epoxide group of epoxy resin which is on prepreg and forming ether and ester linkage [11] (Figure 1.5). In this way, we can improve interlayer adhesion by means of covalent bonding.

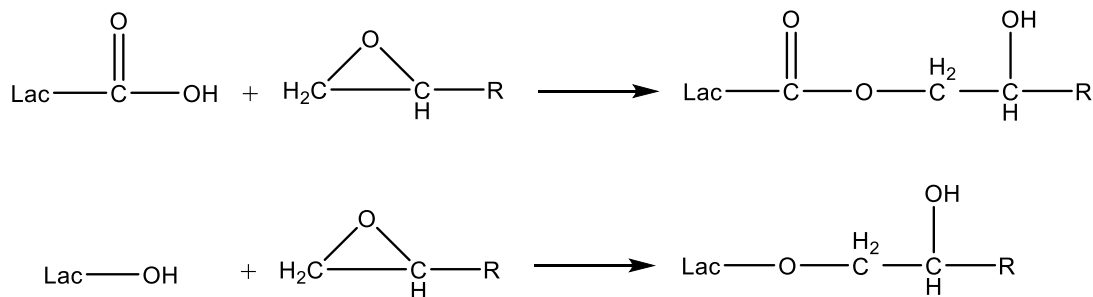


Figure 1.5 Reaction between shellac and epoxy resin.

In addition, PTMC thermoplastic elastomer is chosen as a third polymer for our system. It can add some elasticity to interface and balance between matrix and nanofiber. For effective toughening, intermediate interfacial strength should be

beneficial. Because if it is too strong due to shellac and epoxy interaction, the result is excessive debonding of nanofibers from matrix thus decreases in G_{IC} mode.

In addition, PCL thermoplastic polymer was selected for improving G_{IC} without any chemical bonding. Balanced interdiffusion of PCL could provide sufficient adhesion and create strong resistance in G_{IC} owing to better load transfer to nanofibers.

All these polymers were used in interleaving mats. And aim of this study is to evaluate the contribution of micro scale (void nucleation, fiber debonding, crack pinning and fiber pull-out) and nano scale (shellac bridging) mechanisms on interlaminar fracture toughness of laminates.

CHAPTER 2

BACKGROUND AND LITERATURE SURVEY

2.1. Composite Materials

In general, the composite material is made up of two or more different constituents which have notably distinct properties in terms of mechanically, chemically and physically. However; when these different properties are combined, better properties rather than those of individual constituents are possessed. They have begun to be used in many industrial areas in order that they have excellent features like high strength and stiffness, wear resistance, lightweight, thermal conductivity, corrosion resistance, fatigue life, thermal insulation and so on.

Composite materials are composed of a continuous phase known as matrix and a filler phase also called reinforcement (Figure 2.1) [12].

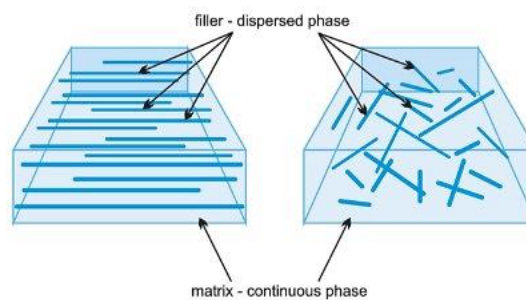


Figure 2.1 Phases of composites. [13]

Matrix phase is used as a binder material. This phase has to be continuous so that it could be support and protect filler phase from the environment like moisture and chemicals. Also, it has a role of transferring stresses to the fillers. Generally, filler

phase has higher density, strength and stiffness than matrix. In this way, it provides composite to a stronger structure [13]. Moreover, reinforcements improve properties of composite like thermal expansion co-efficient, and conductivity.

2.1.1. Classification of Composite Materials

Whereas there are a few methods to categorize composite materials, most common classification is based on their matrix and reinforcement constituents as indicated in below Figure 2.2. By means of nature of matrix, they are divided into three main classes; Polymer Matrix Composites (PMCs), Metal Matrix Composites (MMCs) and Ceramic Matrix Composites (CMSs). By the different reinforcement phase, composites are grouped into fiber-reinforced composite, particle-reinforced composite and structural composite materials.

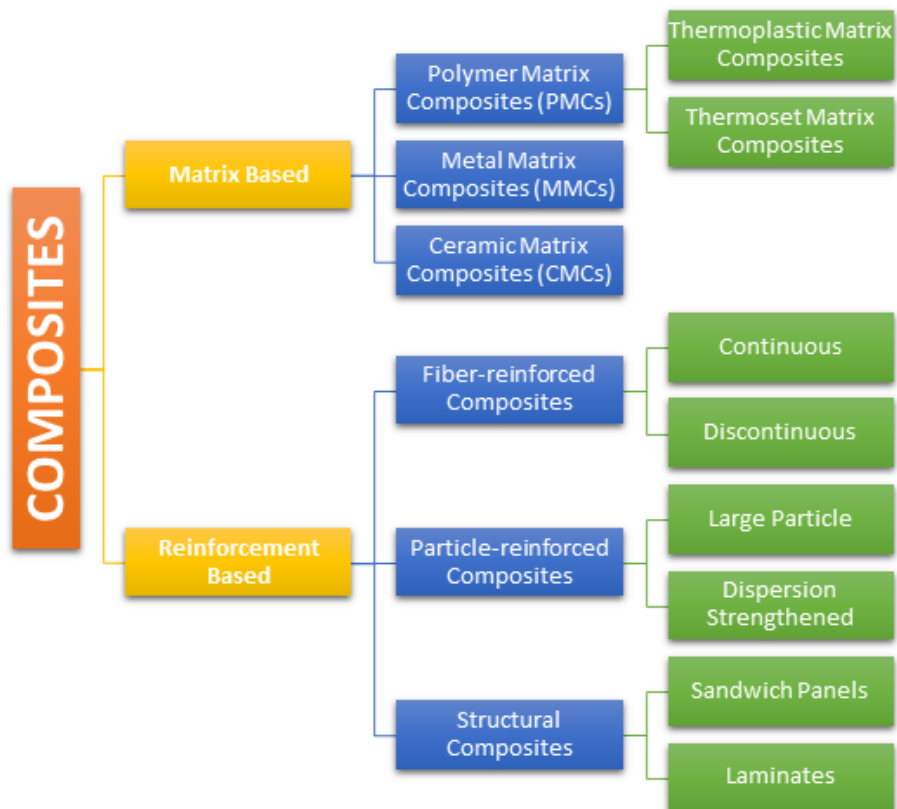


Figure 2.2 Classifications of composites based on matrix and reinforcement.

Matrix and filler phases could be chosen with respect to performance needs of the desired composite and its usage condition. Table 2.1 summarizes some types of composites and their application areas.

Table 2.1 Composite types, their properties and applications.

	Type	Property	Application Area
Matrix	Ceramic [14]	Light weight, excellent creep resistance, high temperature strength	Civil aircraft application
	Metal [15], [16]	Good thermal and electrical conductivity, good wear and heat resistance	Automotive and marine industry
	Polymer [17]	Low weight, high strength, corrosion resistant.	Rocket nozzles, wind turbines, wheelchairs, brake pads for aircraft.
Reinforcement	Fiber [18]–[21]	High-temperature material, low weight/high stiffness, good chemical resistance	Aerospace and aircraft industry, marine application, automotive industry, sporting goods industry
	Particle [22], [23]	Quickly hardened, fracture resistant, strong	Concrete, cements, dental applications
	Structural [24]	Excellent stiffness to weight ratio, capable of absorbing large amount of energy.	Automotive, aerospace, marine, civil and aeronautical applications

2.1.2. Advantages and Disadvantages of Composites

In addition to composite's advantages, they have also some disadvantages when compared to other materials. Table 2.2 shows the summary of pros and cons of composites [25].

Table 2.2 Pros and cons of composites.

Pros	Cons
Light weight, high strength	Very expensive
High degree of freedom in material and process	Cannot be easily repaired
Corrosion and chemical resistance	UV-sensitive
Fatigue resistance	Recycling process not developed enough.
Possible design to requirements (strength, stiffness, thermal resistance etc.)	Finishing not well-developed.

2.1.3. Composite Laminates

Composite laminates are getting reputation in a wide variety of industries like aerospace, marine, sports gear, automotive and many other applications. Especially, carbon fiber reinforced plastic laminates are considered as the new base high-performance composite material due to their high performance and mechanical properties [26]. Most of this type of laminates are made up of pre-impregnated fibers which is also known as prepreg (Figure 2.3).

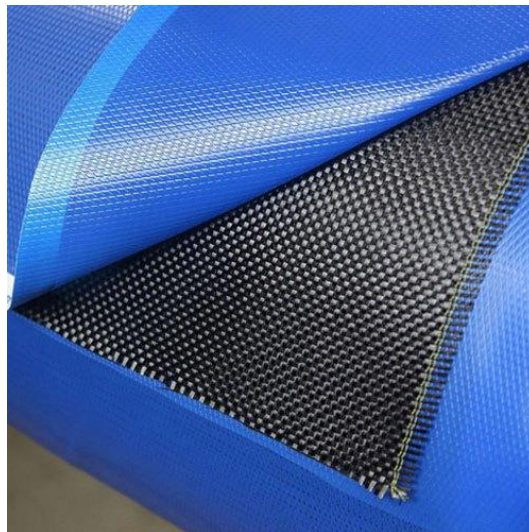


Figure 2.3 Carbon fiber prepreg. [28]

Mostly, prepreg has a combination of fiber reinforcement and highly viscous matrix. Prepreg could be unidirectional form (one directional reinforcement) and fabric form (several directions of reinforcement). In order to prevent complete polymerization and, help for ease of handling, the resin matrix of prepreg which is generally epoxy, is partially cured and conserved in a cold place. To obtain full polymerization, heating process will be needed [27].

For tailoring (stiffness, strength, thermal stability), composite laminates are produced by placing prepregs at desired place with desired angles. Also, the desired composite thickness could be obtained by placing few plies of prepreg.

If a lay-up is made up of a single ply or plies with same orientation, this is called as lamina. However, if plies are bound with different angles, this lay-up is called as laminate [28]. The layers of a laminate generally have various orientations in between -90° and $+90^\circ$. Laminate sequences are represented by $[a/90/b/c/0/d/\dots]$. Here, “a” shows the first ply orientation, “90” shows the second ply orientation, and so on.

For instance, $[45/0/-15/90/45]$ is a five-ply laminate [29]. Figure 2.4 represents stacking of prepreg plies to a laminate with different angles of fibers [30]. Various fiber orientations and stacking sequences affect structural response, failure and damage mechanism of composite laminates.

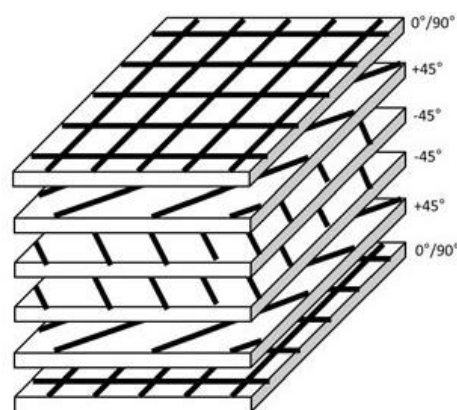


Figure 2.4 Stacking of prepreg plies to a laminate with different angles of fibers. [32]

2.1.4. Failure and Damage Mechanisms for Composite Laminates

When the structure loses its function, this situation could be called as a failure. There are some criteria in order to designate the failure mechanism. These are stiffness, yielding fatigue life, impact resistance, bending, corrosion resistance and so on. On the other hand, laminates failure mechanism is a precious case since before laminates rupture completely, they have some local failures and these local failures are called as damage. The list which includes damages mostly occurred in composites is given below.

- Splitting
- Buckling
- Fatigue
- Impact damage
- Creep and stress relaxation
- Delamination

Splitting- When the fibers run in one direction and adhesion latitudinal to fiber direction, splitting could be occurred in composite laminates. Some cracks will be developed parallel to fibers direction. Generally, in-plane bending and a wedge effect in a bearing or connection are the reasons of this failure mechanism [25].

Buckling- Without considering type of material, buckling could be seen at a low applied stress and causes big deformation on the composite laminate [31]. Buckling in composite laminates often leads to delamination damage on the composite. To overcome buckling failure mechanism, more rigid structure will be needed. Moreover, by means of reducing length and using thicker layer might be helped to this problem [25].

Fatigue- Like in steel, fatigue causes damage in composites. However, failure mechanism is a bit different than those of steel. In steel material, crack is caused due to varying loads repeated continually and it grows further by effect of alternating loads. The structure of steel is broken when the crack length achieved its critical value.

On the other hand, in composite laminate, there are numbers of fatigue cracks and they could develop at the same time in various directions. These cracks might be combined and cause great cracks and delamination [25].

Impact damage- Generally, it is hard to see and detect the damage from impacted surface of composite laminates because of their elastic behavior.

Creep and stress relaxation- In composite laminates, fibers transport the load, and relax the stress on resin. As a result, creep will take place. Creep behavior is highly affected by higher temperature and other environmental conditions [25].

Delamination- When two neighbor plies of the composite laminate separate from each other, this is called as delamination. It is the most crucial failure mechanism for laminates because it highly affects durability and damage tolerance of composite material.

2.2. Delamination

Delamination (Figure 2.5) [32] is the one of the most crucial failure mechanism and evaluation of this failure is important to understand damage tolerance of composites. Delamination is a sneaky failure mode since it is generally invisible and not detected by visual inspection. It has adverse effects on stiffness and strength of composites, therefore; lifetime of material is reduced when delamination is occurred.

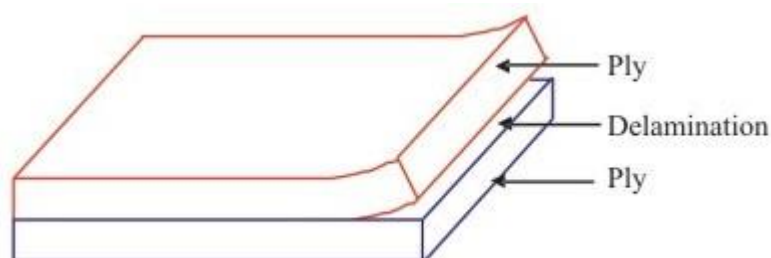


Figure 2.5 Delamination failure mechanism. [34]

2.2.1. Delamination Modes

Delamination could grow under three basic modes (Figure 2.6); crack opening mode (Mode I), sliding shear mode (Mode II) and scissoring shear mode (Mode III). Also, delamination could develop in the mixed-mode which is composed of various combination of these three basic modes.

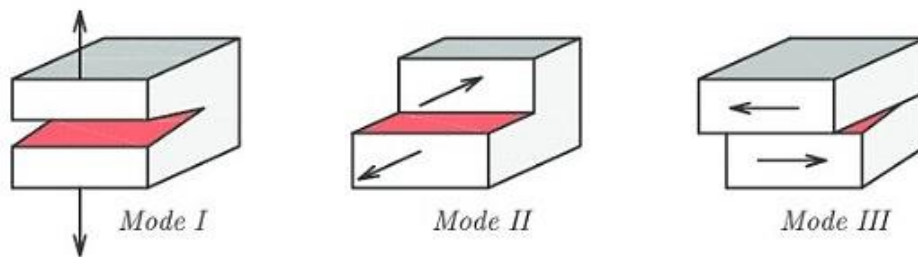


Figure 2.6 Modes of delamination. [35]

The critical energy strain rate which has symbol with G_C , is mostly known as total required energy to begin delamination failure in material. Each delamination modes have its own G_C values, i.e., G_{IC} for Mode I, G_{IIC} for Mode II and G_{IIIC} for Mode III. Different test methods are used to measure all these values.

Mode I: The double-cantilever beam (DCB) test is mostly used for determination of G_{IC} (the interlaminar fracture toughness in mode I) and recently, this test is standardized by American Society for Testing and Materials (ASTM). Test specimen is shown in Figure 2.7.

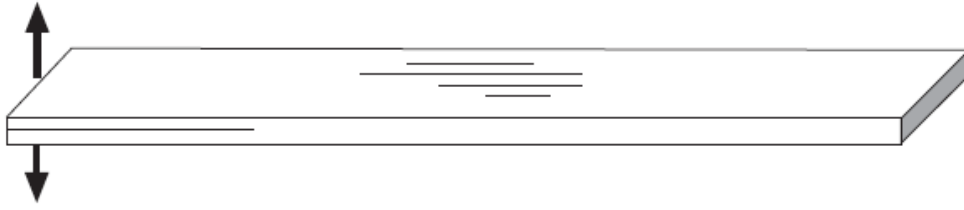


Figure 2.7 The geometry of DCB test specimen. [36]

Mode II: The end notched flexure (ENF), the stabilized end notched flexure (SENF), the four- point end notched flexure (4ENF) and the end loaded split (ELS) test specimens could be used for measuring the interlaminar fracture toughness in Mode II. Among them, the end notched flexure (ENF) test has been widely used to predict pure mode II delamination result. Figure 2.8 represents the geometries of Mode II test specimens.

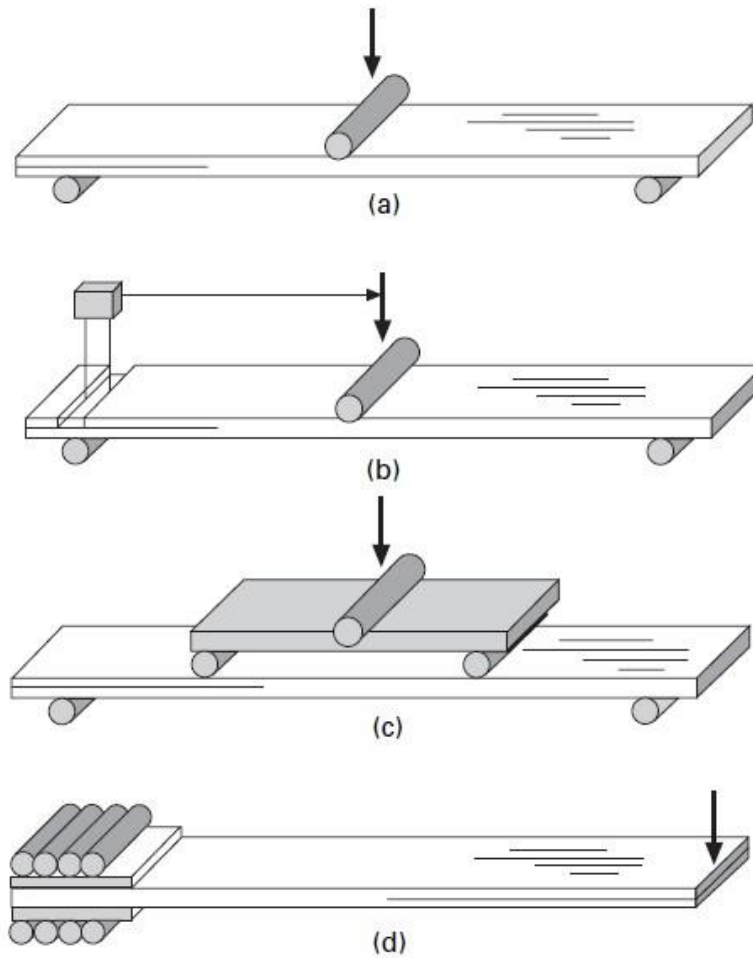


Figure 2.8 The geometries of Mode II test specimens; (a) ENF; (b) SENF; (c) 4ENF; (d) ELS. [36]

Mode III: The split cantilever beam (SCB) test is used to measure the interlaminar fracture toughness in Mode III. However, calculation of pure Mode III delamination is quite difficult. Studies of Martin [33] and Donaldson [34] shows that pure Mode II results could not be obtained with the SCB test. The edge crack torsion (ECT) test has been used to get pure G_{IIIc} value. The geometries of test specimens for Mode III measurement are shown in Figure 2.9.

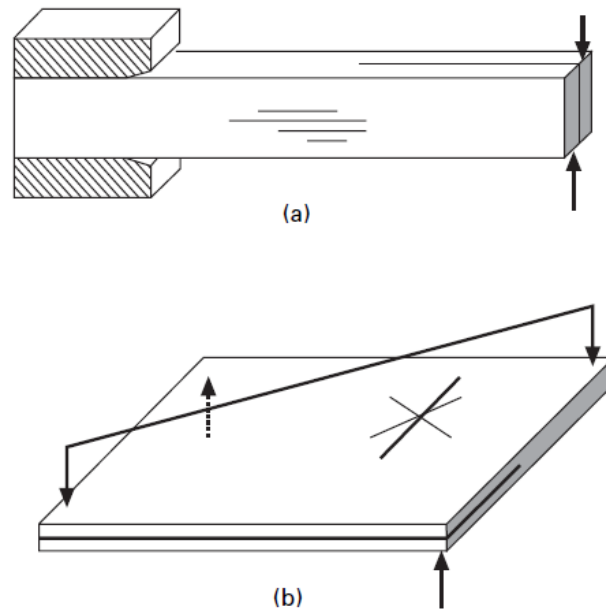


Figure 2.9 The geometries of specimen for Mode III tests; (a) SCB; (b) ECT. [36]

Mixed-Mode: There are six widely used test methods for calculating mixed-mode fracture toughness value. These are the mixed mode bending (MMB), the mixed mode flexure (MMF), the cracked lab shear (CLS), the single leg four point bend (SLFPB), the asymmetric DCB (ADCB) and the Arcan. Generally, MMB specimen has been used for the mixed-mode. All mentioned test specimens' geometries are in Figure 2.10.

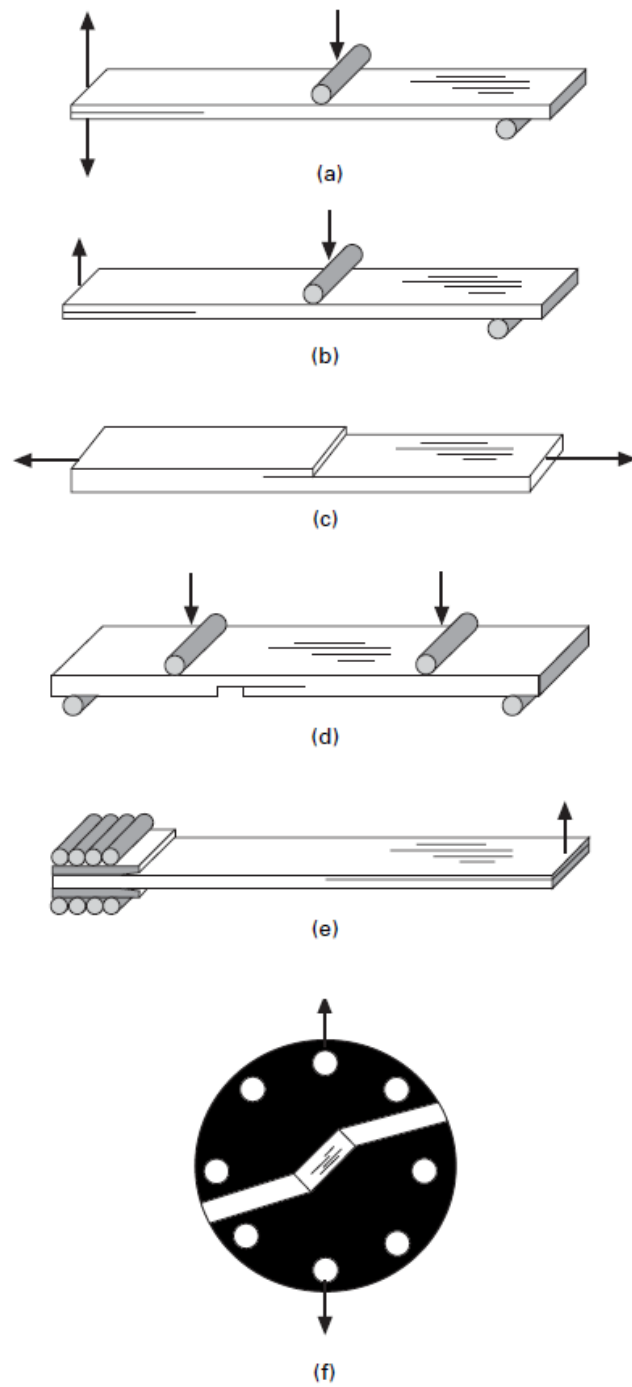


Figure 2.10 The geometries of specimen for Mixed-Mode tests; (a) MMB; (b) MMF; (c) CLS; (d) SLFPB; (e) ADCB; (f) the Arcan. [36]

2.2.2. Sources of Delamination

Discontinuities in composite structure are the most common reason of delamination because they lead to increase on interlaminar stresses [36]. Figure 2.11 represents main sources of these discontinuities.

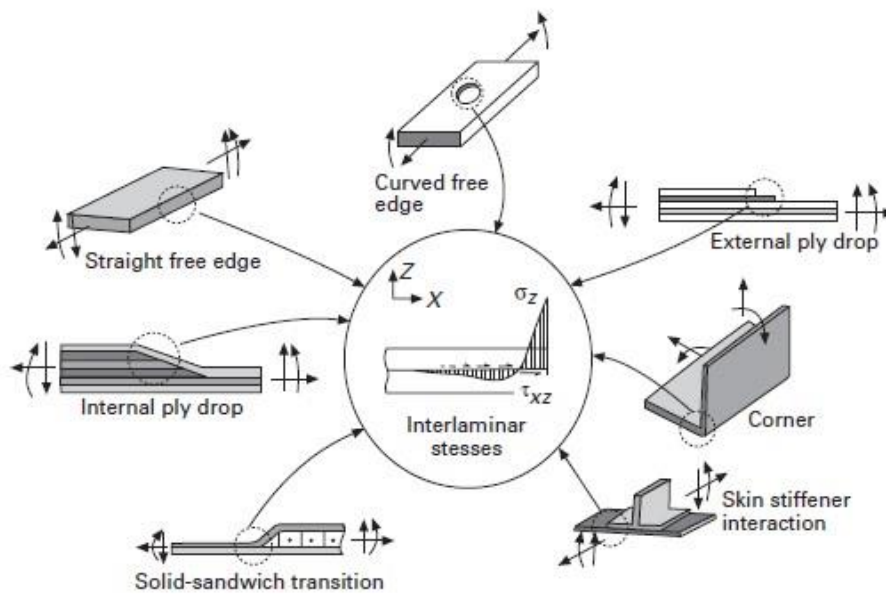


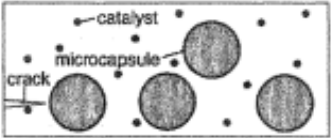
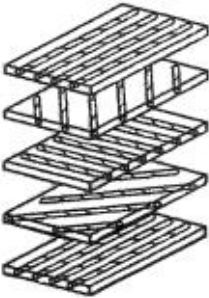
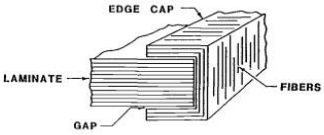
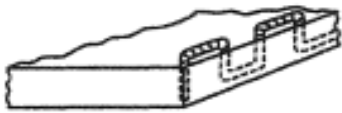
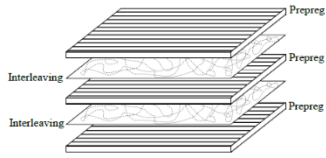
Figure 2.11 Sources of delamination. [36]

Because of unaligned peculiar layers, delamination may take place at stress free edges. It also happens at region where the thickness of material is decreased. In addition, delamination occurs at bending area. All failure modes generally occur in case of delamination.

2.2.3. Proposed Solutions to Delamination Failure

Nowadays, designers have a great concern for finding new constructions in order to restrain delamination in material structure. Most of researchers have been dealing with understanding and preventing breakdown mechanism behind of delamination. All of these studies have a contribution to improvement on delamination failure by means of developing materials and their constructions. Decreasing interlaminar stresses and increasing fracture toughness are essential points for healing delamination. In light of this concept, there are numerous approaches to heal delamination failure and improve the performance of laminate composites over the years. Matrix toughening [35], optimization of stacking sequences [36], edge cap reinforcement [37], through-thickness stitching [38] and ductile interleaving are shown as an example of such kind of researches. However, each solution mechanism also has some limitation and Table 2.3 summarizes limitation of proposed solution mechanisms.

Table 2.3 Summary for limitation of proposed solution techniques.

	Methods	Disadvantages
	Matrix toughening	Decrease overall shear modulus and lose in glass transition temperature (T_g) of resin.
	Optimization of stacking sequences	May not work when applied load is inverted.
	Edge-cap reinforcement	High manufacturing cost and enhance rigidity
 <p>STITCHING</p>	Through-thickness stitching	Adverse effects on strength and fatigue life of laminates
	Ductile interleaving	Increase in weight and decrease in-plane mechanical properties

First attempt is the modification of the chemistry of the resin composites. In this way, fracture toughness of resin is raised when compression strength of composite is still same. In this technique, at least one component is added to resin base and added component should have lower shear modulus than that of resin base. According to study conducted by J. Verrey [35] et al. in 2005, the hyperbranched polymers (HBPs) is used to modify resin in order to enhance interlaminar toughness of carbon/epoxy composite laminate. With the addition of 7.5% HBP into epoxy resin, G_{IC} value is raised from 600 J/m^2 (for pure epoxy resin) to 750 J/m^2 . On the other hand, modified epoxy resin causes poor fiber-matrix interfaces and in order to heal this functionality problem, amine is added to modified epoxy resin. Figure 2.12 illustrates the configuration of amine groups, HBPs and epoxy chains. As a result, both the problem caused by poor matrix-fiber interface is solved and G_{IC} values increases from 750 J/m^2 to 1400 J/m^2 . However, amine groups addition to interface could be disadvantageous because it lowers glass transition temperature of resin from $184 \text{ }^\circ\text{C}$ to $150 \text{ }^\circ\text{C}$.

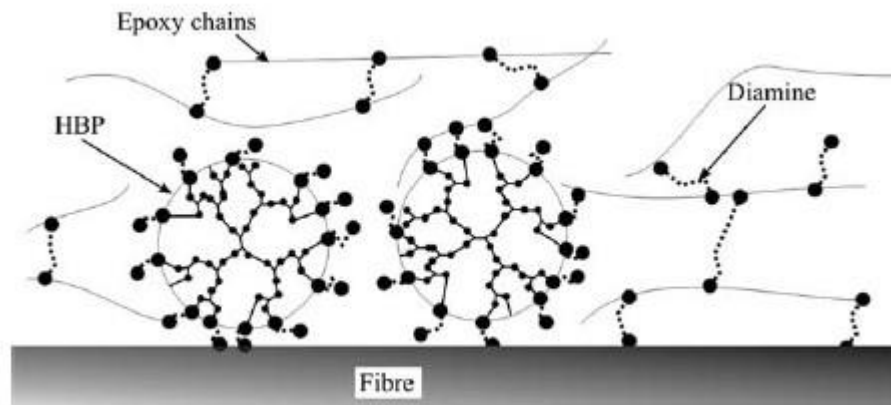


Figure 2.12 The configuration of amine groups, HBPs and epoxy chains. [39]

Another approach of healing delamination is to change stacking sequences of plies. With this technique, there may be a change in the interlaminar or intralaminar strength in laminate composite. Therefore, failure caused by delamination could be lowered or

prevented. On the other hand, this solution does not work when the applied load on composite laminate is inverted since the stress on the laminate is also inverted [36].

Edge cap reinforcement by means of packing the edges of laminate composites is another preventing solution for delamination. The study conducted by Howard [37] shows that with edge capping technique, interlaminar stresses is lowered and fatigue strength is increased. Nevertheless, this technique could be costly and, also enhance the rigidity of laminate in bending aspect.

Through-thickness stitching helps for resisting out-of-plane tensile strength and preventing delamination growth. In case of any impact, stitching holds together plies of laminate and mostly suppress delamination; however, it has negative effect on the fatigue life of laminates which are mainly composed of fibers [38].

All the proposed solutions and designs mentioned above have a reduction in delamination, but have also important enhancement in weight, cost and some loss of in-plane stiffness and strength. By the way, ductile interleaving is a favorable method for both solving these problems and delamination. Figure 2.13 illustrates three main constituents which are used as an interleaving material. These are particles, film and nanofibers.

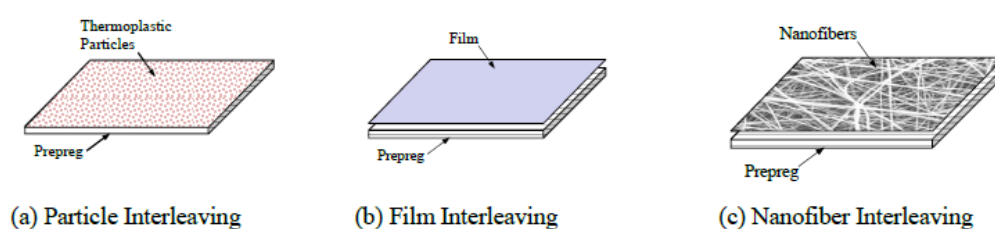


Figure 2.13 Constituents used in interleaving. [43]

According to Hojo's [39] study related with particles interleaving, polyamide particles with a commercial name of T800H/3900-2 was used to enhance interlaminar strength of laminate composite. Carbon fiber/epoxy laminate was used for this study. Schematics of cross section of interleaved laminate is shown in Figure 2.14.

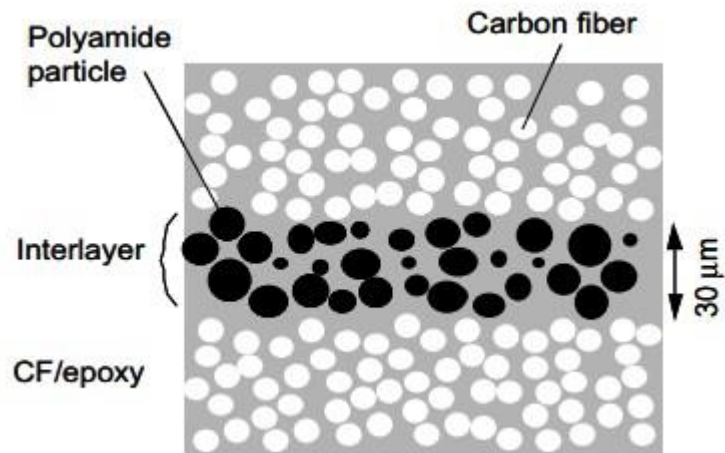


Figure 2.14 Representation of cross section of laminate with particles interleaved. [44]

Polyamide particles interlayer was put into each layer of laminate composite. DCB test was used to measure G_{IC} values of T800H/3900-2 laminate (particle interleaved) and T800H/3631 laminate (reference). Figure 2.15 indicates the results for G_{IC} measurements. G_{IC} initiation value of particle interleaved laminate is approximately four times greater than that of reference laminate.

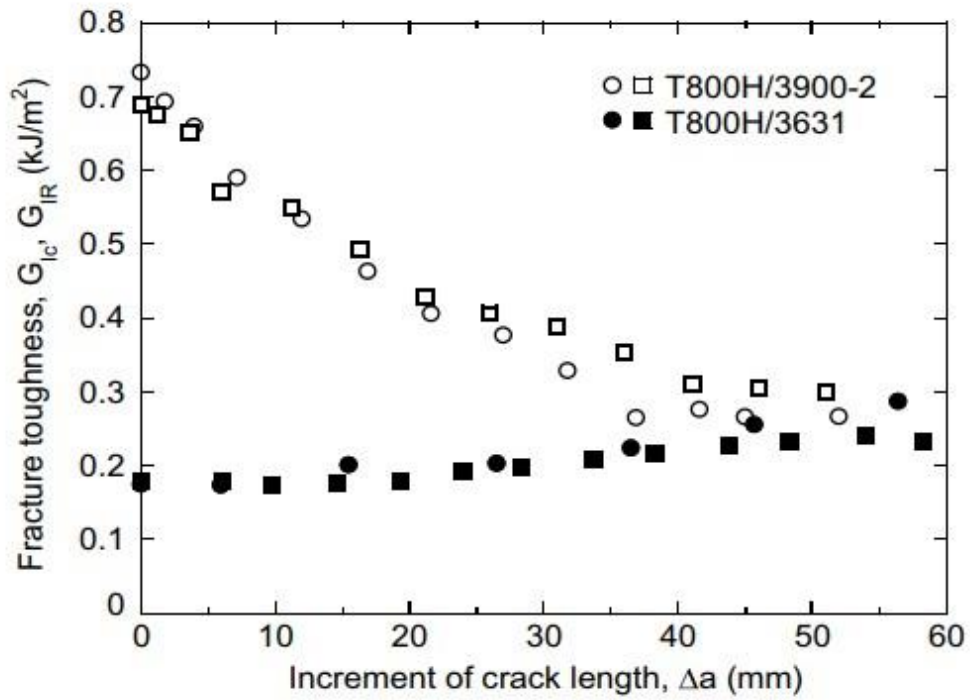


Figure 2.15 Relationship between fracture toughness and increment of crack length for T800H/3900-2 particle interleaved laminate and T800H/3631 reference laminate. [44]

The other outcome of Hojo's study is that delamination is developed in toughened region with particles and crack path grows to untoughened region which is interface of interlayer and base lamina (Figure 2.16).

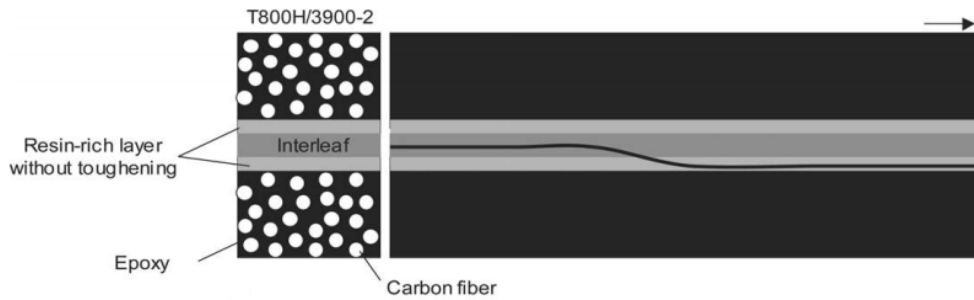


Figure 2.16 Crack path during Mode I measurement. [44]

However, this approach has a limitation such that there is an increase in thickness by up to 30%. This may lead to decrease in-plane mechanical properties of composite. Moreover, particle interleaving has a potential of lowering glass transition temperature.

As distinct from particle interleaving, film interleaving gives an opportunity to make blends of different polymers with different features. Hojo [39] et. al. in 2006 was used the ionomer film as a film interleaving material at the only midplane of laminate which made up of carbon fiber/epoxy prepregs of Toho UT500/111 via hot press. Films with thickness of 25 μm and 100 μm were used in this study. Figure 2.17 illustrates the representation of laminate cross section with film interleaved.

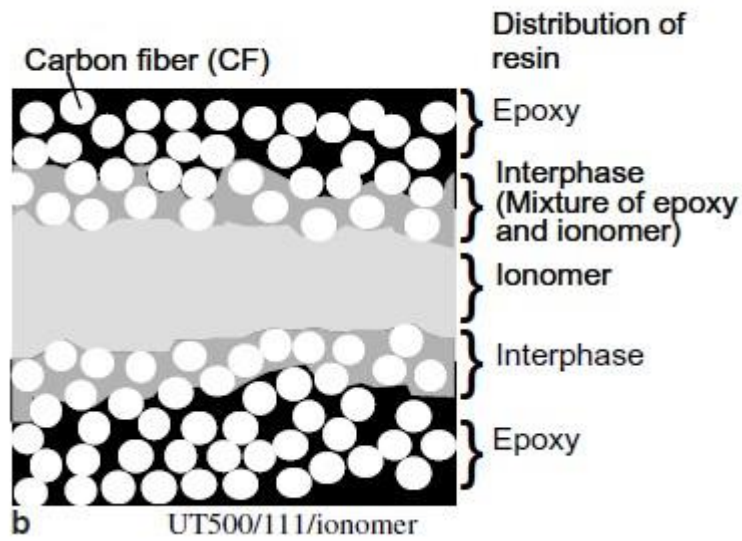


Figure 2.17 Representation of laminate cross section with film interleaved. [44]

According to DCB test results (Figure 2.18), G_{IC} fracture toughness values are increased with film interleaving when compared to G_{IC} value of base laminate. In addition, Figure 2.18 also shows that when the film thickness increases, G_{IC} fracture toughness also increases.

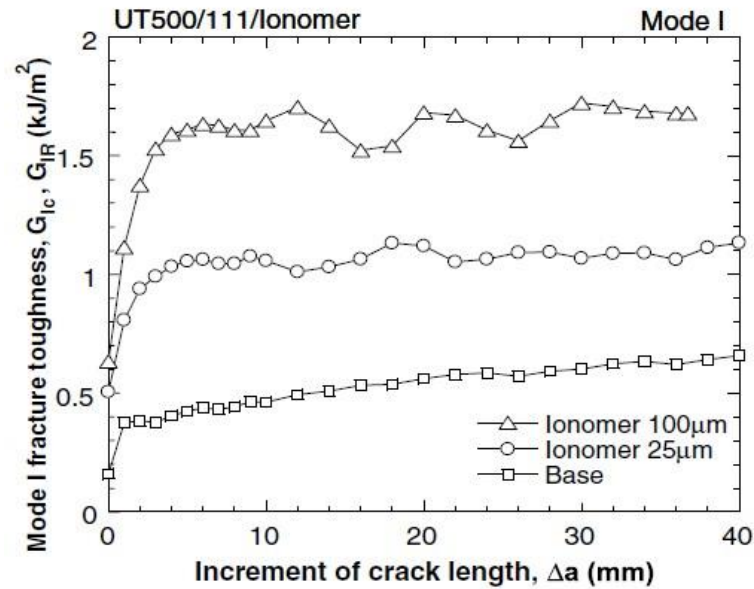


Figure 2.18 Relationship between fracture toughness and increment of crack length for UT500/111/Ionomer film interleaved laminates and UT500/111 base laminate. [44]

Both particles and film interleaving methods have a significant improvement on G_{IC} fracture toughness by means of enhancing interlaminar toughness and decreasing rate of delamination growth; however, interleaf used in these techniques has a higher thickness approximately 20-50% of single ply. As a result of this, laminate thickness is also raised and most probably, reduction in in-plane mechanical properties of laminate is occurred.

As an alternative for these two interleaving techniques, nanofibers is a promising material in this regard because nanofibers could eliminate all the limitation caused by other interleaving techniques like loss of in-plane stiffness and strength, increase in weight of laminate, no complication in production sequence and change in glass transition temperature.

According to study conducted by Shivakumar [40] et al. in 2009, using nanofibers as an interleaving material in composite laminates enhances fracture toughness,

damping, fatigue delamination growth while there is no significant change in weight and in-plane mechanical properties of composite.

In Shivakumar's study, Nylon 6,6 polymer was selected for production of nanofiber. Laminate is composed of 20 layers of prepregs. Two layers of nanofiber mat are placed in bottom and top layer of 10th layer of prepregs. Reference laminate was named as AS4/3501-6 and laminate with nanofiber mat was named as interleaved AS4/3501-6 composite. Figure 2.19 demonstrates G_{IC} fracture toughness of neat and nanofiber interleaved AS4/3501-6 laminates. With interleaving process, fracture toughness of composite is increased by approximately 1.5 times.

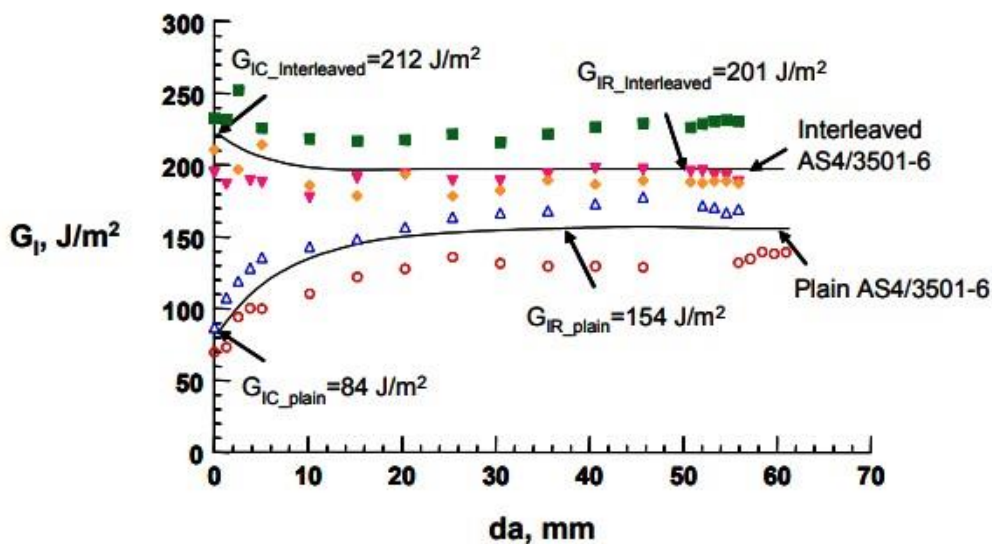


Figure 2.19 Graph of fracture toughness versus crack length of base and interleaved AS4/3501-6 composites. [45]

Nowadays, researchers and designers are still working on this approach to heal delamination. Most important point of using nanofiber as an interleaved layer is that nanofiber polymer and resin which are used in laminate production should be

chemically compatible. If not, required chemical bonding for elongation and fiber bridging are not provided; therefore, this approach is not enough to heal delamination.

2.3. Electrospinning

Electrospinning is the most preferred method in order to produce nanofibers because of its simplicity and ability to generate non-woven nanofiber mats with high surface to volume ratio. Thanks to large surface area of electrospun nanofibers, they could be used in many different application areas such as, tissue engineering, catalysts, biosensors, automotive sector, defense industry, biomedical applications and so on.

It also enables to produce uniform and long nanofibers with different size and shapes. Generally, diameters of electrospun nanofibers are ranging from hundreds of nanometers to micrometer. Huge range of polymers from natural to synthetic could be used in production of nanofibers with electrospinning.

Electrospinning setup is composed of three main equipment which are syringe pump with variable needle (single, double or co-axial), high voltage power supply and metallic collector (planar, grooved, patterned or rotating). Basic schematic diagram of this setup is illustrated in Figure 2.20.

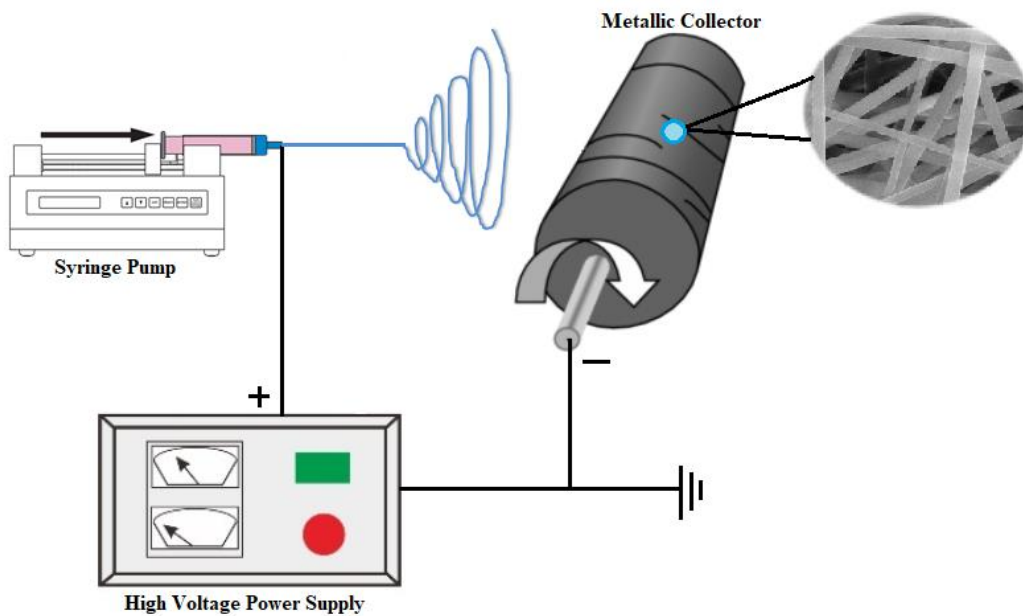


Figure 2.20 Schematic of experimental setup for electrospinning.

During the electrospinning process, air conditioner is mostly used in order to maintain room humidity and temperature constant. High voltage (the range a few tens of kilovolts in DC) is applied between metallic collector and syringe tip which is generally a needle. Thanks to electrostatic forces between these two, droplet of polymeric solution at the tip of the syringe is turned to a conical shape which is known as Taylor Cone. The dominance of electric field is greater than the surface tension of polymeric solution, solution is ejected to metallic collector. When the solution jet is flying in air, solvent in the polymeric solution evaporates and leaving nanofibers behind. In consequence of this, charged nanofibers are collected on metallic ground.

2.3.1. Parameters for Electrospinning

Electrospinning process could be affected some parameters (Figure 2.21) and these parameters are categorized into three groups:

- Ambient condition parameters
- Polymer solution parameters
- Process condition parameters

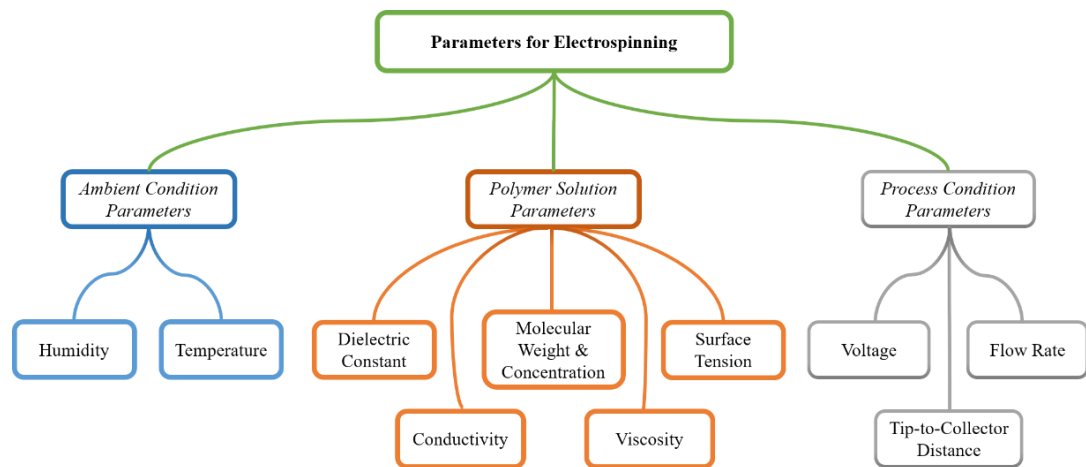


Figure 2.21 Parameters for electrospinning.

Humidity: Kim [41] et al. in 2004 conducted a study which showed that fiber diameter increases when relative humidity in electrospinning chamber air increases. Moreover, it affects fiber morphology by means of affecting evaporation rate of solvent. During evaporation stage of solvent in electrospinning process, high humidity causes some solvent inside the jet when it reaches the ground collector. After all solvent evaporates, pores are created on the surface of the fibers.

Temperature: It affects both viscosity of solution and the evaporation rate of solvent. Increasing temperature causes decreasing viscosity of solution and increasing the evaporation rate of solvent. Therefore, fiber diameter decreases [42].

Dielectric constant: When the dielectric constant of solution enhances, solution could store more charges. This leads to more elongation of polymeric jet, then nanofiber diameters are lowered. The study conducted by Lee [43] et al. in 2003 states that poly(ϵ -caprolactone) (PCL) is insoluble in N,N-dimethylformamide (DMF), but soluble in methylene chloride (MC). However, dielectric constant of DMF is higher than that of MC. Therefore, addition of DMF into polymeric solution of PCL in MC increases the total dielectric conductivity of polymeric solution. As a result of this, smaller diameter nanofibers are produced in this case.

Conductivity: To form nanofiber, jet should be stretched by means of repulsion of the charges at polymeric droplet. When the conductivity of the polymeric solution is raised, charges on the jet are also raised. Sometimes, charges on the jet are not enough to stretch electrospinning solution to get smoother and finer nanofiber. In that case, some salt could be added in solution to increase jet charge and cause to higher elongation on the polymeric jet. Therefore, less bead and more finer nanofiber formation are achieved [44].

Molecular Weight and Concentration: If low molecular weight polymers are used in electrospinning, bead formation could be occurred because molecular weight of solution is related with the number of chain entanglement which has a crucial role for spinnability of polymer solution [45]. Moreover, molecular weight of polymer influences concentration of solution as well as solution viscosity. In the study of Ki et al. [46], there is a correlation between concentration and fiber diameter. When the concentration of the electrospinning solution increases, fiber diameter also increases.

Viscosity: As mentioned before, solution viscosity is affected by solution concentration. Increasing solution concentration means that increasing solution viscosity. For the determination of fiber morphology, viscosity is the most crucial parameter. Beads are formed instead of nanofibers at low viscosity (or concentration) because the polymeric solution is spread, and the name of this process is called as electro spraying. On the other hand, at high viscosity (or concentration) polymeric

solution droplet may dry at the tip of need, then optimal viscosity should be found in order to produce continuous and linear nanofibers.

Surface tension: For the initiation of electrospinning process, surface tension of the liquid jet should be less than intensity of the electric field. Some solvents with low surface tension may be added to polymeric solution to lowered surface tension of electrospinning solution and then produce fiber without beads.

Voltage: There is a correlation between applied voltage and electrostatic repulsive forces. According to study conducted by Megelski [47] et al. in 2002, only by increasing spinning voltage, fiber diameter is decreased while all other parameters kept constant.

Flow rate: The flow rate of solution affects bead size and fiber diameter because volume of solution ejected towards to collector increases with increasing flow rate. Bead size and fiber diameter proportional to flow rate of the solution.

Tip-to-collector distance (TCD): It has an effect both the travelling time of jet and electric field strength on the jet. When TCD is lowered, electric field strength increases and travelling time of solution jet decreases. Therefore, the solvent in solution jet does not have enough time to evaporate before reaching the grounded collector. On the other hand, when the TCD is increased, solution jet elongates more and have more time to reach grounded collector. Thus, fiber diameters will be smaller [44].

2.4. Polymers Used in Nanofiber Production for Interfacial Toughening (IFT)

The main reason of the preference of nanofibers as an interleaving agent is that nanofibers help to decrease stresses caused by mismatching plies. They also play a role as a bond between plies with keeping the weight and in-plane mechanical properties of composite same. In the literature, many different polymers have been used in production of nanofibers for the aim of using interleaving material in composite laminates. Some examples are polysulfones (PSF) [48], poly (vinylidene

fluoride) (PVDF) [49], poly (vinyl alcohol) (PVA) [50], polyvinyl butyral (PVB) [6], poly(ϵ -caprolactone) (PCL) [3], [51] and polyamide (PA) [3]. These polymers have distinct mechanical behaviors as well as chemical structures. All these factors affect the adhesion between fiber and epoxy. Nanofibers with all types of polymer have significant effects on mechanical behaviors of composite laminates such as fatigue strength, impact resistance, damage resistance, fracture toughness and so on. Table 2.4 summarizes results of studies' effects on G_{IC} fracture toughness.

Table 2.4 Polymers used in IFT and their effects on G_{IC} .

Polymers used in IFT	Changes in Mechanical Properties
Polysulfones (PSF) [48]	280% improvement in G_{IC} compared with reference (without nanofiber) laminate
Poly(vinylidene fluoride) (PVDF) [49]	G_{IC} improved by 43% for initiation and 36% for propagation stages.
Poly(vinyl alcohol) (PVA) [50]	G_{IC} improved by 65% for initiation and 73% for propagation.
Polyvinyl butyral (PVB) [6]	G_{IC} improved by 53% for initiation and 16% for propagation.
Poly(ϵ -caprolactone) (PCL) [51]	G_{IC} improved by 92% for initiation and 34% for propagation
Polyamide 6 (PA6) [3]	Slightly or no increase in G_{IC} .

Daelemans [3] et al. in 2016 worked with PA6 and PCL nanofibers for IFT of composite laminates. According to working result, PCL has significant effect on both G_{IC} and G_{IIC} fracture toughness values. On the other hand, PA6 has a great improvement on G_{IIC} fracture toughness value, but slightly or no changes in G_{IC} fracture toughness. Figure 2.22 illustrates graphical representations of study's result.

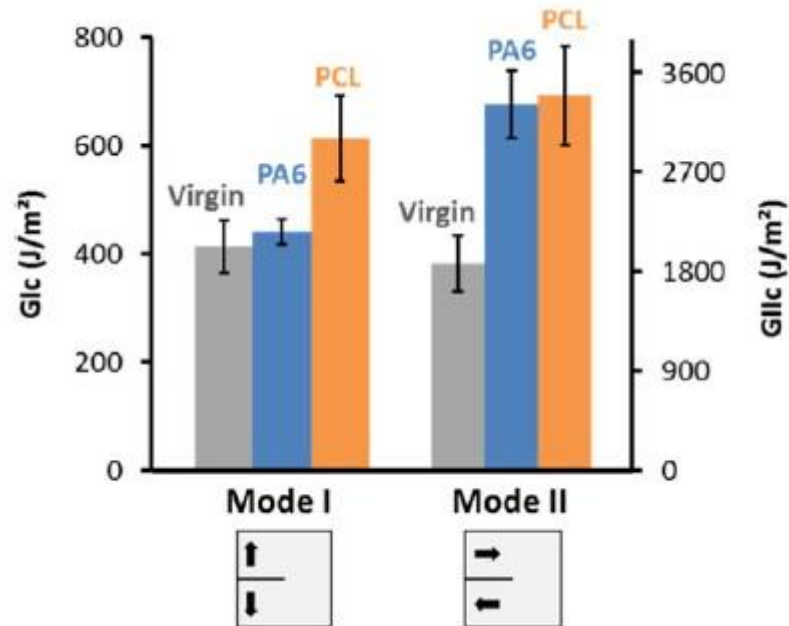


Figure 2.22 Comparison of G_{IC} and G_{IIC} values for PCL and PA6 nanofibers interleaved composites and reference composite. [3]

After Mode II loading, both PA6 and PCL nanofibers form bridging zones and nanofibers straining during impact loading. Thanks to this straining, G_{IIC} of both interleaved composite laminates are enhanced. SEM micrographs of fracture surfaces (Figure 2.23) represent bridging zone and straining of nanofibers.

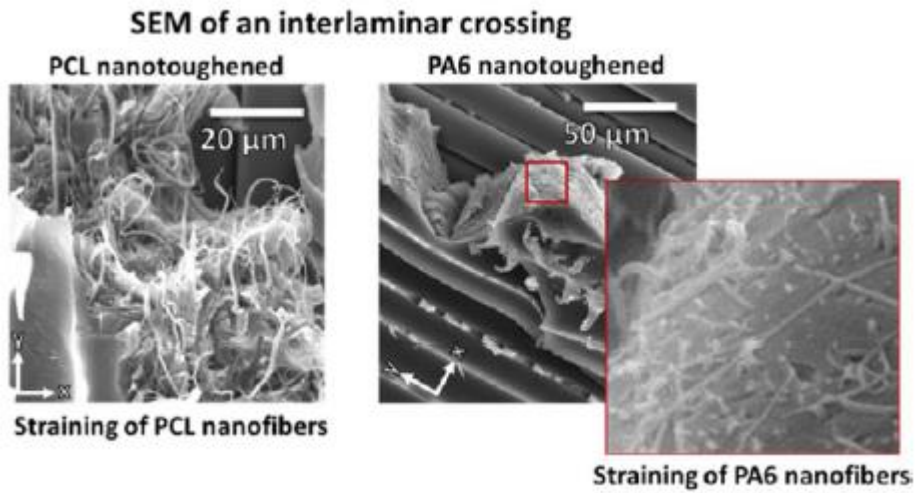


Figure 2.23 SEM micrographs of fracture surfaces composites interleaved with PA6 and PCL nanofibers after Mode II loading. [3]

Moreover, SEM analysis of fracture surfaces after Mode I loading of these composites (Figure 2.24) revealed that PCL nanofibers form bridging zone and this could be led to debonding and breakage of nanofibers. This contributes to improvement on fracture toughness. Nevertheless, PA6 nanofibers interleaved composite's fracture surface micrographs show peeling of nanofibers due to low adhesion between nanofibers and epoxy matrix.

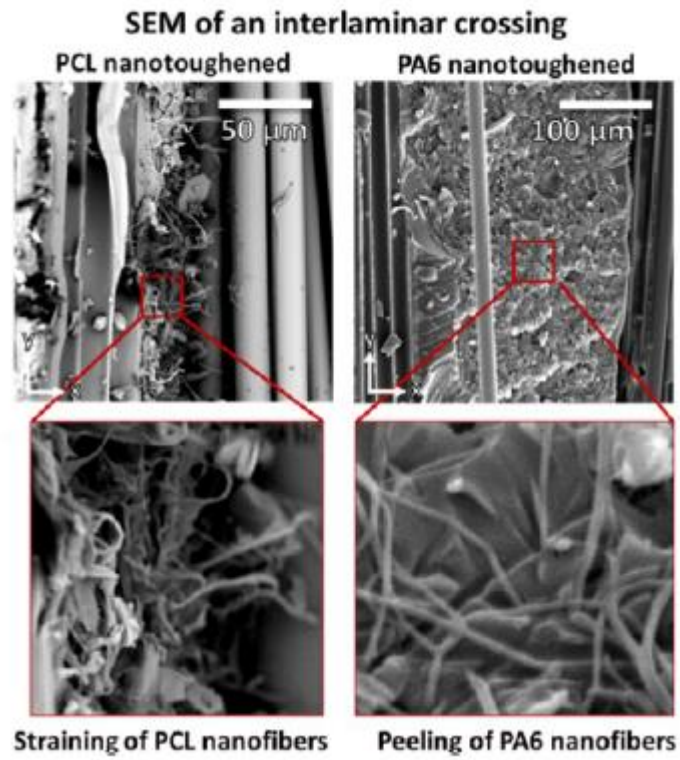


Figure 2.24 SEM micrographs of fracture surfaces composites interleaved with PA6 and PCL nanofibers after Mode I loading. [3]

By looking these results, further investigations are needed about the interlaminar fracture toughness enhancement on G_{IC} with PA6 nanofibers.

CHAPTER 3

MATERIALS AND METHODS

3.1. Materials

Shellac was kindly supplied by Aklar Kimya. 1,6-hexanediol was supplied from VWR. Trimethylene carbonate (1,3-dioxan-2-one, TMC) was supplied from Huizhou Foryou Medical Devices Co., China. Stannous octoate (tin 2-ethylhexanoate, Sn(Oct)₂) was purchased from Sigma Aldrich. Polyamide 6 and poly (ϵ -caprolactone) were supplied from Aldrich. Ethanol and 2,2,2-trifluoroethanol (TFE) were purchased from Merck. VTP H 300 CFA 200 3KT RC42 HS carbon fiber prepreg was obtained from SPM Kompozit. Prepreg has 200 g/m² 2x2 carbon fiber and 42% (w%) epoxy. Mechanical properties of prepreg was listed in Table 3.1.

Table 3.1 Mechanical properties of prepreg.

Carbon Fiber Properties	Tensile Modulus	249 GPa
	Tensile Strength	4518 MPa
	Density	1.79 g/cm ³
	Strain	1.7 %
Epoxy Properties	Fracture Toughness	0.7-0.8 MPa√m
	Fracture Energy	130-170 J/m ²
	Density	1.19 g/cm ³

Table 3.2 Solution contents in terms of solvent and polymer type.

Solutions	Electrospinning		Electrospraying	
	Polymer(s)	Solvent	Polymer(s)	Solvent
ES-1	PA6	TFE	-	-
ES-2	PA6-Shellac	TFE	-	-
ES-3	PA6-Shellac	TFE	-	-
ES-4	PA6-PTMC	TFE	-	-
ES-5	PA6-PTMC-Shellac	TFE	-	-
ES-6	PA6-Shellac	TFE	-	-
ES-7	PA6	TFE	Shellac	Ethanol
ES-8	PA6-PCL-Shellac	TFE	-	-
ES-9	PA6-PCL	TFE	Shellac	Ethanol
ES-10	PA6-PCL	TFE	Shellac	Ethanol

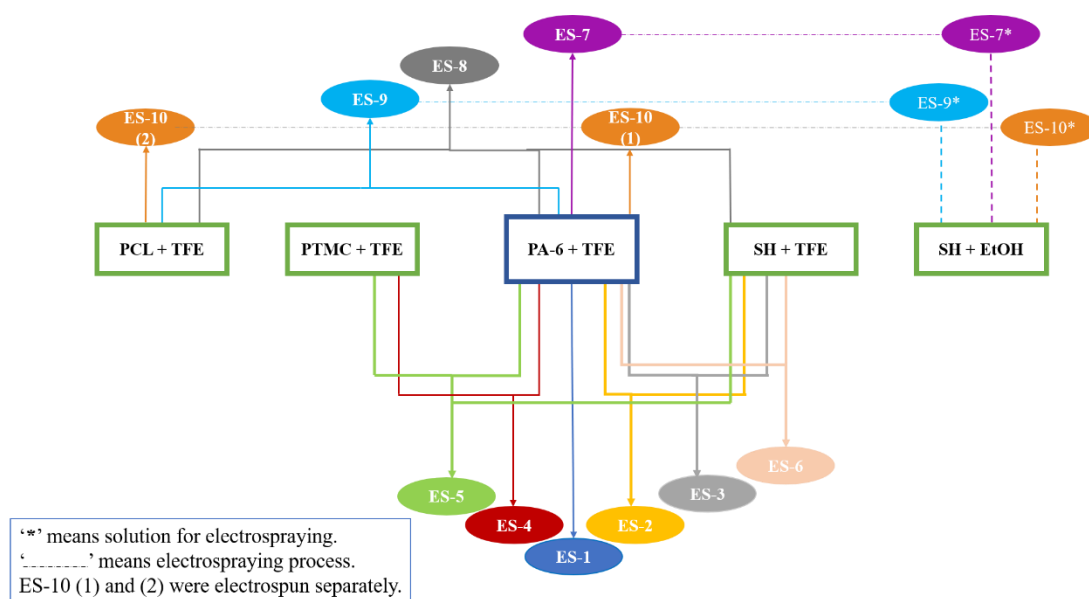


Figure 3.2 Flow chart for preparation of solutions.

Firstly, each polymer was dissolved in its corresponding solvent and stirred until completely dissolved. Then, to get the electrospinning solution, each polymer solutions were mixed and then stirred overnight. On the other hand, electrospaying

solution was prepared separately and not mixed to electrospinning solution. To illustrate, for the preparation of ES-9, 0.94 g PA6 was dissolved in 4.8 mL TFE and stirred until all the polymer particles dissolved. Same procedure was applied to 0.63 g PCL in 5.5 mL TFE. When polymers were dissolved very well, these two polymeric solutions were mixed and stirred overnight to get a homogeneous solution. In the meantime, 3 g shellac was dissolved in 9 mL ethanol separately from other two mixtures. This solution was not added to PCL+PA6 polymeric mixture because it was used in electrospaying process. Amount of solute and solvent were determined by trial-and-error method in order to get optimum concentrations to be able to perform electrospinning process properly. Appendix B includes detailed information about contents of each electrospinning and electrospaying solutions.

3.2.3. Production of Nanofibers via Electrospinning

In this work, experimental setup shown in Figure 3.3 was used for electrospinning and electrospaying processes. Four parameters were kept constant throughout the whole study. One was tip-to-collector distance which was 20 cm. The second one was diameter of needle (18 AWG). The needle moved on horizontal axis along the collector length in order to get homogeneous distribution of nanofibers and beads on both axes. The third parameter was speed of moving needle which is 1 cm/s. The last one was the rotating metallic collector. It consists of four aluminum discs with a diameter of 13 cm. It rotated at 100 rpm for all productions. An oxidized copper plate was used to cover aluminum discs as a collector surface (see in Figure 3.4).

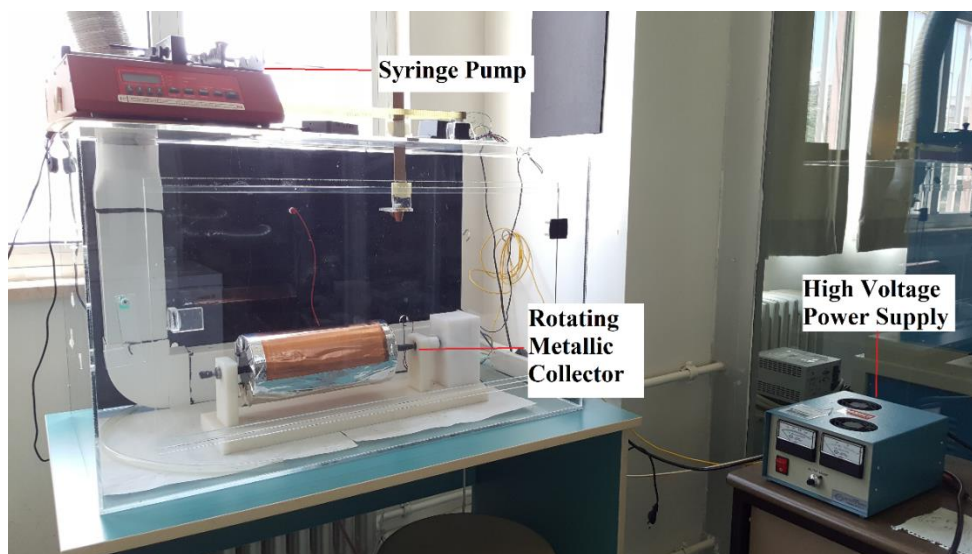


Figure 3.3 Experimental setup for electrospinning and electro spraying.



Figure 3.4 An oxidized copper plate.

For spinnability, optimum voltage and flow rate values of each solution were listed in Table 3.3. In order to transfer same amount of polymer to each composite interlayer, 0.7 g nanofiber veil was put as a target. Then, required spinning or spraying time was calculated for each process according to equation shown below (Equation-1). Detailed information for each electrospinning solution were found in Appendix B.

Equation-1;

$$t = \frac{100 \times y}{v_{\text{solution}} \times \rho_{\text{solvent}} \times S}$$

Where;

t: required spinning or spraying time in terms of hour

y: amount of polymer (g) that could be collected as nanofibers

v_{solution} : flow rate of solution (mL/h)

ρ_{solvent} : density of solvent (g/mL)

s: amount of polymer found in solution in terms of weight percent.

Table 3.3 Electrospinning/electrospraying process parameters for each ES.

<i>Solution Name</i>	Electrospinning			Electrospraying		
	<i>Voltage (kV)</i>	<i>Flow Rate (mL/h)</i>	<i>TCD (cm)</i>	<i>Voltage (kV)</i>	<i>Flow Rate (mL/h)</i>	<i>TCD (cm)</i>
ES-1	15	1.75	20	-	-	-
ES-2	19.5	1.65	20	-	-	-
ES-3	17.5	1.65	20	-	-	-
ES-4	16	1.65	20	-	-	-
ES-5	17	1.65	20	-	-	-
ES-6	15	1.45	20	-	-	-
ES-7	17	1.5	20	18.5	1.15	20
ES-8	15	1.65	20	-	-	-
ES-9	15	1.65	20	18.5	1.15	20
ES-10	18 (PA6) 21 (PCL)	1.85 (PA6) 1.30 (PCL)	20	18.5	1.12	20

For ES-1, ES-2, ES-3, ES-4, ES-5, ES-6 and ES-8: Nanofiber veils were produced in the same way. Briefly, syringe was filled with electrospinning solution then it was placed into syringe pump. According to Table 3.3, flow rate of solution and voltage were arranged, and electrospinning process was started.

For ES-7 and ES-9: Firstly, electrospaying of shellac was performed onto oxidized copper surface in order to produce nanoparticles. Then, nanofibers were electrospun onto nanoparticles by means of electrospinning. Finally, electrospaying of shellac was performed again and nanoparticles were sprayed over produced nanofiber veils. In this way, sandwich structure represented in Figure 3.5 was obtained.

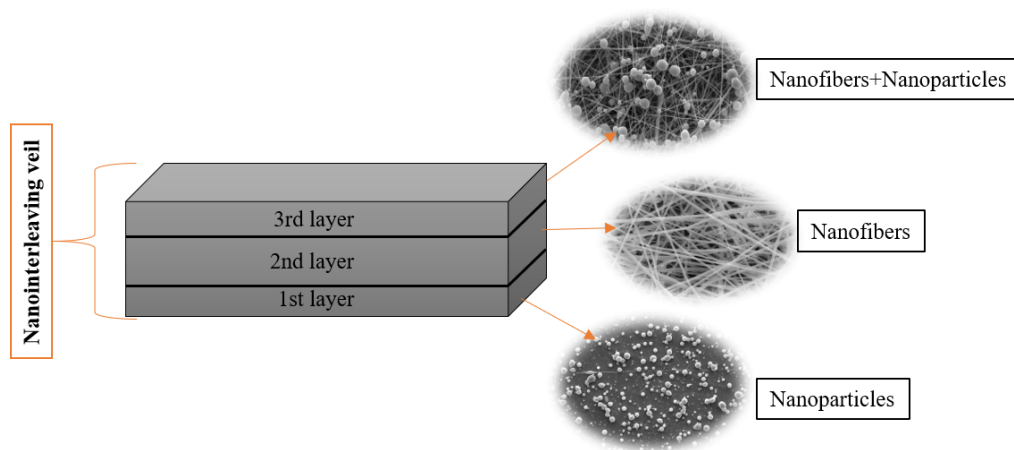


Figure 3.5 Schematic representation of sandwich structure.

For ES-10: Sandwich structure was obtained after finishing production. In the first place, shellac was sprayed on collector and nanoparticles were formed. Then, over them, PA6 solution and PCL solution were electrospun on the same collector at the same time by using two different syringe pumps. After producing the required amount nanofibers, again shellac solution was sprayed over the nanofibers.

3.2.4. Production of Composite Laminates

In this work, prepreg with 215 mm width and 300 mm length was used and composite laminate was produced by stacking 18 plies of prepregs. Teflon tape, 75 μ m thickness, was used to initiate delamination. In the lay-up process, this tape was placed in the mid-interface of prepreg plies along 70 mm. After nanofiber production was done, veil was transferred to interface between the mid-plane of the prepreg layers. Figure 3.6 illustrates this procedure.

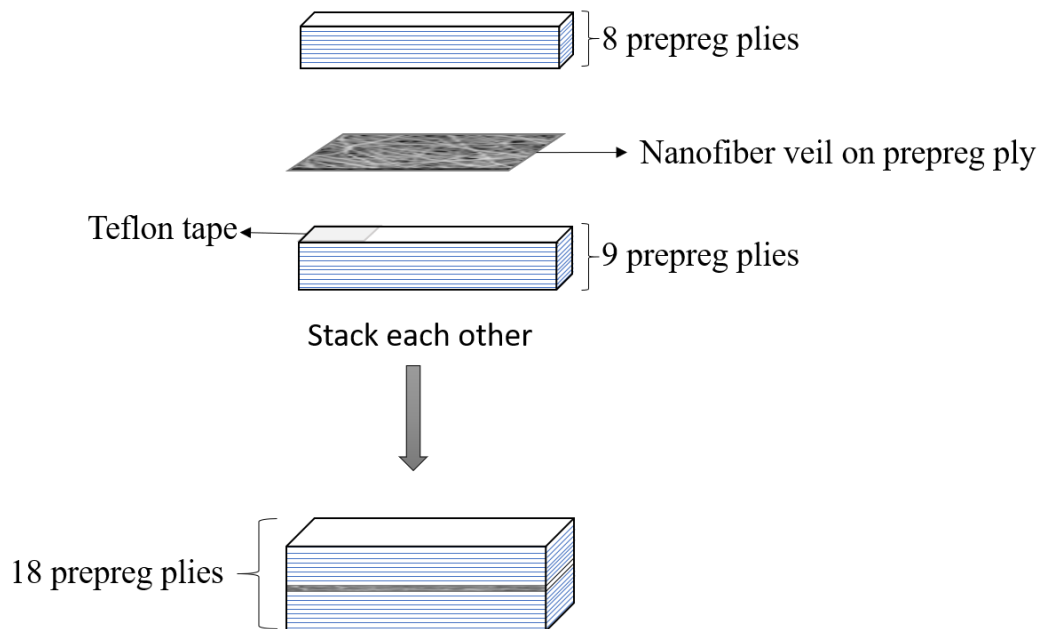


Figure 3.6 Representation of the transferring nanofiber veil to mid-interface of prepregs.

Hot press (Figure 3.7) was used for curing process. Curing procedure was performed at 120 °C and 7 atm. Temperature profile of this procedure is shown in Figure 3.8.



Figure 3.7 Hot press used for curing composite laminates.

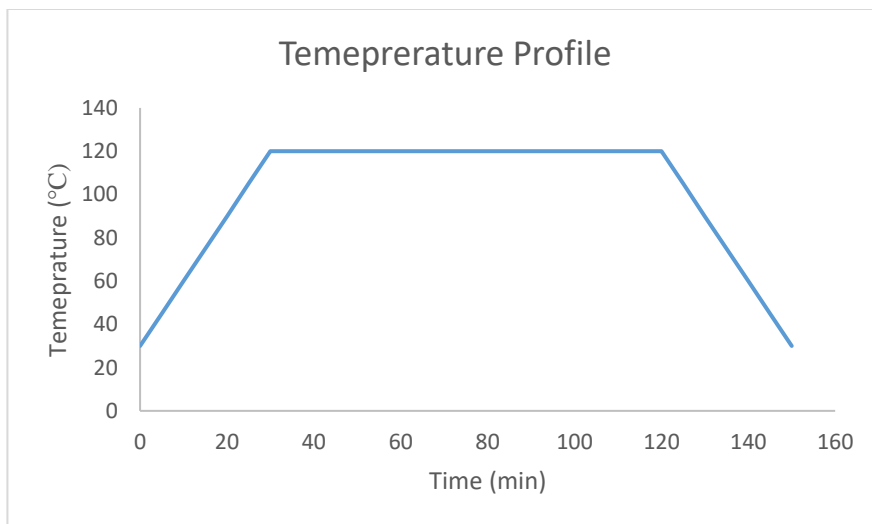


Figure 3.8 Temperature profile of curing process.

After composite production, 6 samples were cut from composite laminate for DCB tests. Each sample has a 3.4 mm thickness, 26 mm width and 275 mm length.

3.3. Characterizations

3.3.1. Gel Permeation Chromatography (GPC)

Molecular weight of two-armed low molecular weight PTMC was determined via Polymer Laboratories PL-GPC 220. Chloroform was used as eluent (1 mL/min flow rate) at ambient temperature.

3.3.2. Scanning Electron Microscopy (SEM)

Bilkent University National Nanotechnology Research Center (UNAM), FEI Quanta 200F SEM instrument was used to analyze morphology of the produced nanofibers and fracture surface of composite laminates after DCB test. Nanofiber veils and fracture surface samples were attached to holders using carbon tape. In order to increase conductivity of fracture surface sample, liquid silver was used in addition to carbon tape. Then, samples were coated with gold-palladium via Precision Etching and Coating System at UNAM.

3.3.3. Double Cantilever Beam (DCB) Test

ASTM D5528 was used as a reference to measure Mode I fracture toughness of composite laminate. Six specimens with dimensions of 3.4 x 26 x 275 mm were cut from produced laminate and each of them was marked with white-out for each side in order to follow crack growth on specimen. Specimen was painted from the last point of Teflon tape. In the first 5 mm, each 1 mm was signed. Afterwards, marking was done for every 5 mm until the crack reached 45 mm. Then, test specimen was fixated

on fixing heads mechanically. Figure 3.9 shows the DCB test specimen with marking and fixing heads.

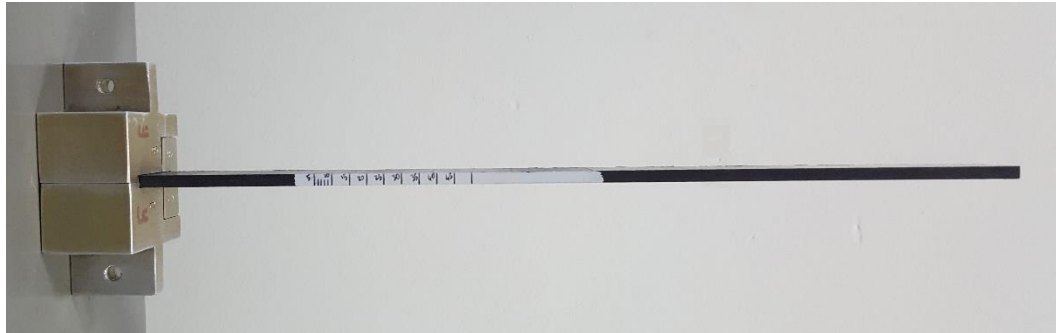


Figure 3.9 The DCB test specimen.

Detailed information about the DCB test procedure is given in Appendix C.

CHAPTER 4

RESULTS AND DISCUSSIONS

4.1. PTMC Synthesis

By means of ring opening polymerization of TMC monomer, polymerization with 500:1 monomer:initiator ratio was carried out at 130 °C for two days to obtain PTMC. Stannous octoate was used as a catalyst in this synthesis. For the determination of synthesized PTMC's molecular weight, GPC analysis was performed and, the number average molecular weight (M_n) was calculated as 53,090 g/mol. The chromatogram of synthesized PTMC was found in Appendix A.

4.2. Production of Nanofibers

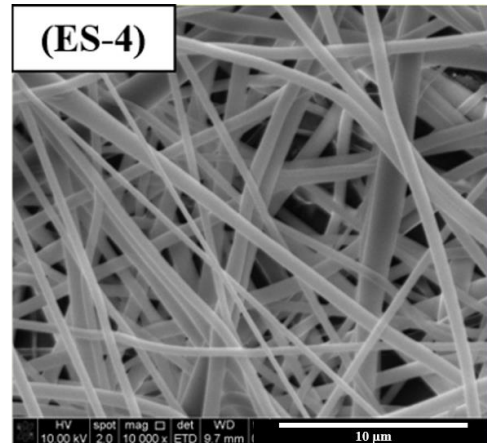
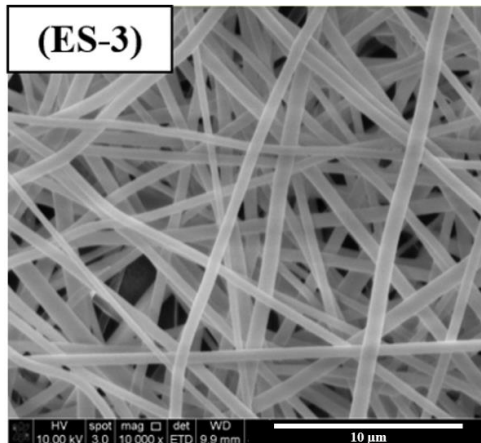
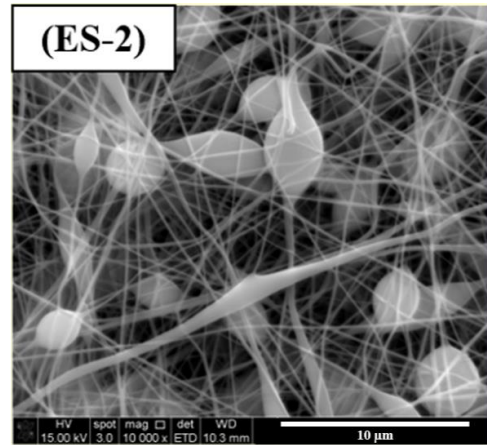
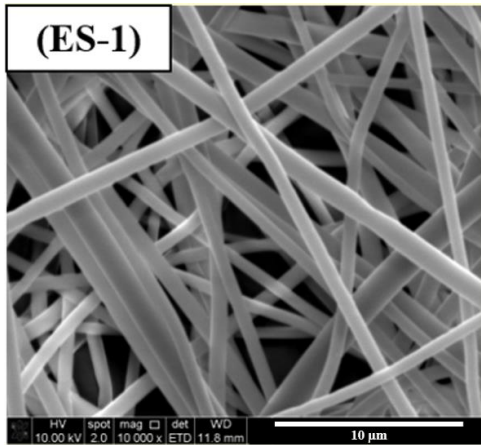
Nanofibers were produced at an ambient temperature of 18-23 °C and a relative humidity of 28-45%. Electrospinning and electrospraying techniques were performed during the production of veils. Produced veils are classified in four groups in order to see the effects of changing parameters. Aim of these groups and included solutions are listed in Table 4.1.

Table 4.1 Veils' groups and their aims.

	Aim of group	Solutions	Difference between solution in the groups
<i>Group A</i>	The effect of shellac and its concentration on G_{IC} .	ES-1, ES-2, ES-3, ES-6	The ratio of polymer in ES-2 and ES-3 The concentration of polymers in ES-2 and ES-6
<i>Group B</i>	The effect of PTMC on G_{IC}	ES-1, ES-4, ES-5	ES-5 contains also shellac
<i>Group C</i>	The effect of PCL on G_{IC} .	ES-1, ES-8	PCL and shellac were added
<i>Group D</i>	The effect of shellac beads on G_{IC} .	ES-1, ES-2, ES-7, ES-9, ES-10	Different production methods for nanoveils.

Firstly, with Group A composites, the aim was to see the effect of shellac on G_{IC} by forming covalent bond with epoxide group of epoxy resin and strengthen interface of laminates. Changing with concentration of electrospinning solutions and weight percent amount of polymer used in nanofiber system were studied. Then, to eliminate excessive reinforcement in laminate interface, PTMC was added to PA6 and shellac nanofiber system due to its elasticity, and also low T_g which helps to make homogenous blend with epoxy matrix during curing process. These types of composites are classed in Group B. Third group, Group C, includes composites produced by nanofiber system which contains PCL in addition to shellac and PA6 polymers. PCL was used for the same reason as in like PTMC. And the last one is the Group D. It is formed to compare the shellac beads effects on the interfacial toughening. In this group, PA6, shellac and PCL were used in different configurations in order to get the highest increment on G_{IC} . Details about each composite are discussed in the following sections.

The morphology of nanofibers and nanoparticles produced by electrospinning and electrospraying were characterized with SEM. SEM micrographs of produced nanofibers and beads are shown in Figure 4.1. Red scale bar represents 10 μm .



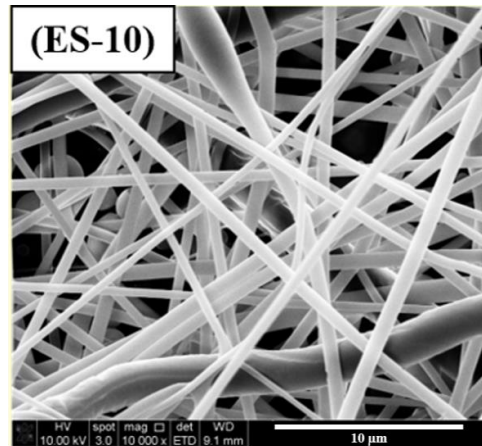
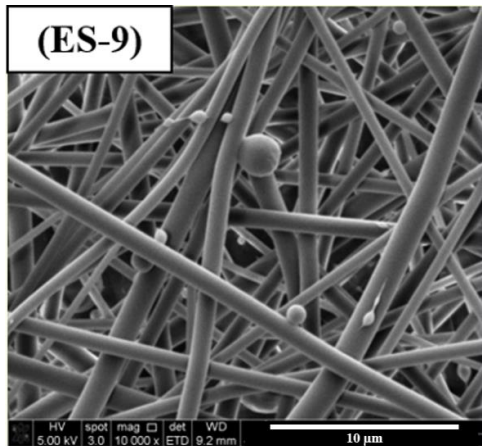
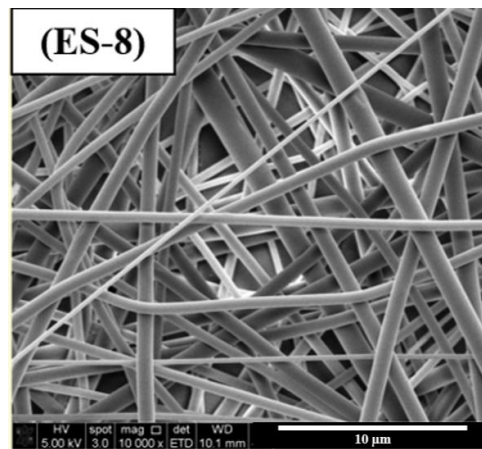
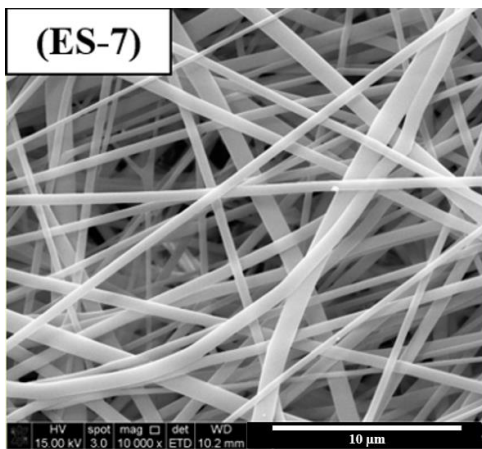
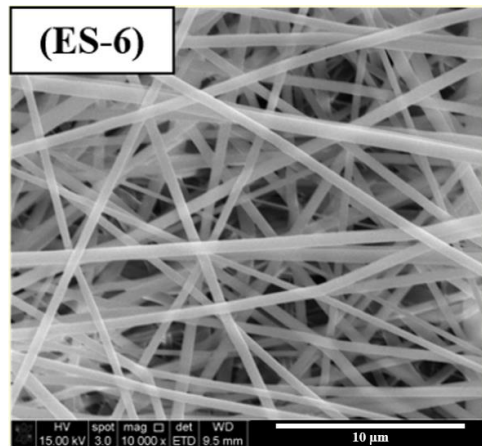
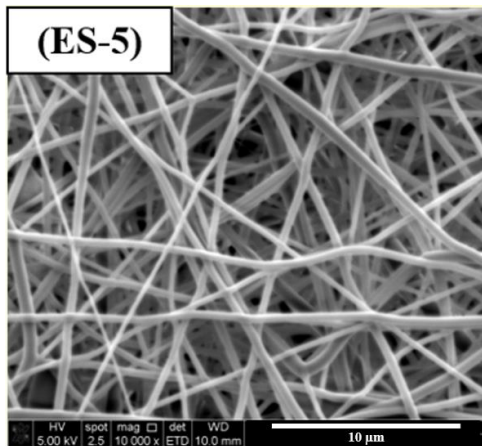


Figure 4.1 Nanofibers SEM micrographs with 10 kX magnification and 10 μm scale bar.

Electrospinning was performed with ES-1, ES-2, ES-3, ES-4, ES-5, ES-6 and ES-8 solutions. Smooth, non-woven fiber formation was achieved with them except ES-2. Nanofibers with beads were obtained by electrospinning of ES-2 solution. To prevent bead formation, ES-6 solution was prepared with the same PA6:shellac ratio as of ES-2 but the overall polymer concentration of the solution was higher for ES-6. The concentration of solution also affects the viscosity of the solution. ES-6 contained PA6 (86%, w/w%) and shellac (14%, w/w%) as like in ES-2. However, the solution had higher concentration values in terms of PA6 and shellac. In ES-2 solution, PA6 and shellac concentration in electrospinning solution are 6.14% (w/w%) and 0.99% (w/w%) respectively ;whereas, these values are 10.63% (w/w%) and 1.72% (w/w%) respectively for ES-6 solution. Then, when the viscosity or concentration of the solution increases, spinnability of the solution mostly increases. With increasing viscosity, nanofibers without beads were could be obtained by electrospinning of ES-6. Moreover, in regard to see the effect of beads on the fracture toughness value of laminate, electrospaying was performed to form beads on the interleaving mat. In the first place, electrospinning of ES-7 solution was performed. Two different solutions were prepared. One was the solution of PA6 polymer in TFE solvent. And the other was the solution of shellac in ethanol. . In the total weight percent of the interleaving mat, PA6 had 86% (w/w%) and shellac had 14% (w/w%) as in like nanofiber mats produced by ES-2 and ES-6. With these solutions, firstly, electrospaying of shellac solution was done and shellac nanoparticles were formed. Then, nanofibers were produced by PA6 solution over the nanoparticles. Again, by means of shellac in ethanol solution, electrospaying was performed over PA6 electrospun nanofibers. Schematic representaiion of this process is shown in Figure 4.2.

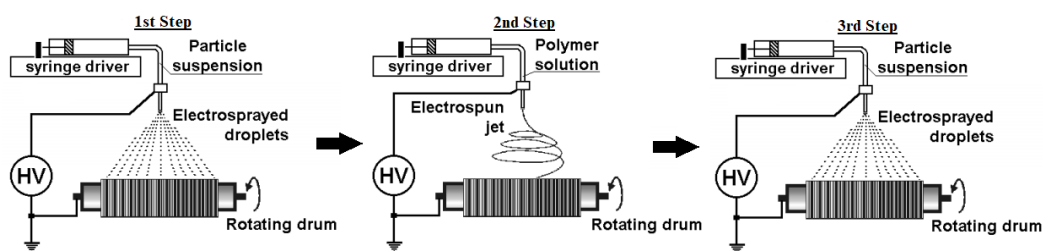


Figure 4.2 Representation of process for ES-7 and ES-9. [57]

Ethanol was chosen as a solvent for electrospinning process because if TFE was used as a solvent in electrospinning process, PA6 nanofibers might be affected and morphology of nanofibers was mostly damaged due to the dissolving nanofibers during evaporation of solvent. PA6 does not dissolve in ethanol. Therefore, in electrospinning process, ethanol did not affect PA6 nanofiber morphology.

In SEM micrograph of ES-7 in Figure 4.1, only formation of nanofibers was observed. Beads formed by electrospinning over nanofibers were not seen from this micrographs. However, shellac nanoparticles produced by the first step of electrospinning was observed in the SEM micrograph in Figure 4.3.

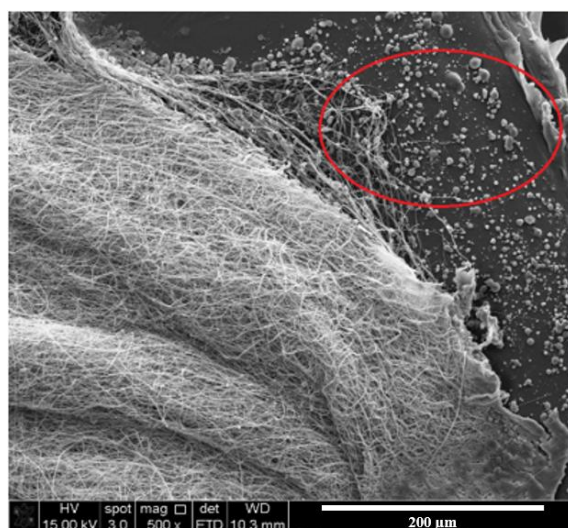


Figure 4.3 SEM micrograph of interweaving mat produced by ES-7.

Also, any shellac particles could not be observed over nanofibers in the SEM micrograph in Figure 4.3. Therefore, we concluded that shellac nanoparticles could not be adhered onto the surface of PA6 nanofibers. During the third step which was electro spraying process, due to rotating of metallic collector, nanoparticles might have spreaded to environment and not be collected on the rotating drum. The same thing is also valid for ES-9.

Polymer content of ES-9 was selected according to previous study [52] which was conducted by Melike Kılıçoğlu under the supervisor of Prof. Dr. Bora Maviş. In this study, the blends of PA6/PCL were studied in the interleaving composite laminates in order to increase fracture toughness. The best result was obtained from the composite which is interleaved with the blend of PA6 and PCL with a percentage of 60% (w/w%) and 40% (w/w%) respectively. In the light of this result, electro spraying of shellac nanoparticles over PA6/PCL nanofibers was performed. ES-9 electro spinning solution contained 60% (w/w%) PA6 and 40% (w/w%) PCL. As the process illustrated in Figure 4.2, electro spraying and electro spinning processes were performed accordingly. Shellac nanoparticles were sprayed as 14 % (w/w%) of total polymer weight in interleaving mat. On the contrary to ES-7, some shellac nanoparticles (shown with red circles) were observed over PA6/PCL nanofibers (Figure 4.4).

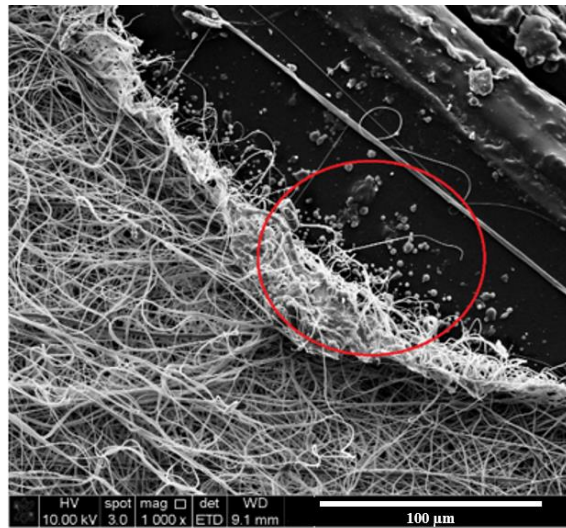


Figure 4.4 The SEM micrograph of ES-9 interleaving mat.

As an alternative approach to ES-9 interleaving mat, ES-10 interleaving mat was produced according to process illustrated in Figure 4.5.

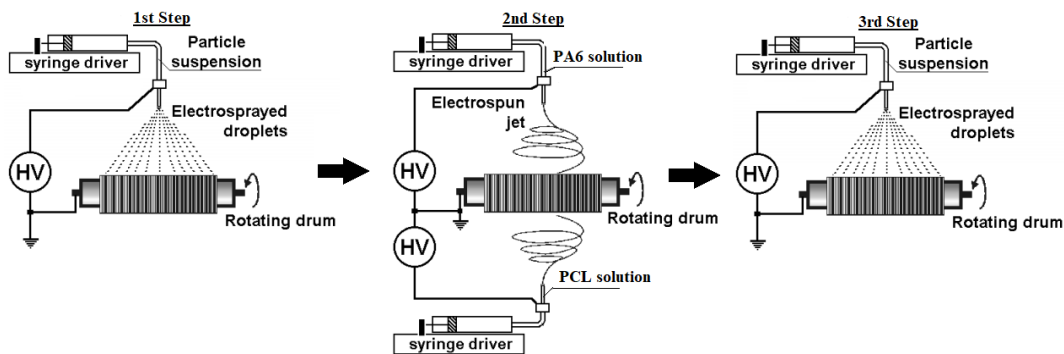


Figure 4.5 Representation of process for ES-10. [57]

Firstly, shellac solution was sprayed to oxidized copper plate as a first layer of interleaving mat, then over nanoparticles, PA6 and PCL solutions were electrospun simultaneously from two different needles. Then, shellac nanoparticles were

electrosprayed over produced nanofibers. Like in interleaving mat of ES-7, shellac nanoparticles were observed only first layer of the interleaving mat for ES-10 (Figure 4.6).

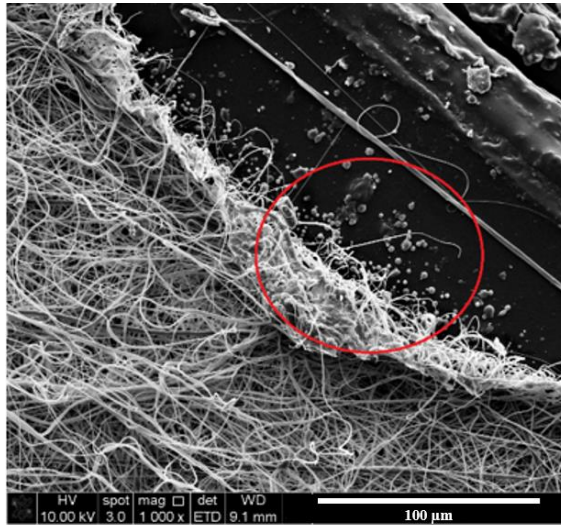


Figure 4.6 The SEM micrograph of ES-10 interleaving mat.

The contribution of all produced interleaving mats to fracture toughness of composite laminates were discussed in Section 4.4. Analysis of Fracture Surfaces.

4.3. DCB Test Results

The aim of this study is to enhance the mechanical performance and behavior of composite laminate by nanofiber interleaving. For this study, Z1 represents reference composite laminate without any interleaving material. In Table 4.2, produced composites are categorized in order to compare between themselves easily.

Table 4.2 Groups and their contents in terms of composite and solution name and polymer used in production.

GROUP A			GROUP B		
COMPOSITE #	ES #	NANOVEIL CONTENT	COMPOSITE #	ES #	NANOVEIL CONTENT
Z2	ES-1	PA6 (100, w/w%)	Z2	ES-1	PA6 (100, w/w%)
Z3	ES-2	PA6:SH (86:14, w/w%)	Z5	ES-4	PA6:PTMC (90:10, w/w%)
Z4	ES-3	PA6:SH (93:7, w/w%)	Z6	ES-5	PA6:PTMC_SH (90:10_3.45*, w/w%)
Z7	ES-6	PA6:SH (86:14, w/w%)			
GROUP C			GROUP D		
COMPOSITE #	ES #	NANOVEIL CONTENT	COMPOSITE #	ES #	NANOVEIL CONTENT
Z2	ES-1	PA6 (100, w/w%)	Z2	ES-1	PA6 (100, w/w%)
			Z8	ES-7	PA Fiber:SH Bead (86:14, w/w%)
Z9	ES-8	PA6:PCL_SH (60:40_3.45*, w/w%)	Z10	ES-9	PA6:PCL_SH Bead (60:40_14*, w/w%)
			Z11	ES-10	PA6 Fiber:PCL Fiber_SH Bead 60:40_14* (w/w%)
(*) means that given shellac ratio is calculated from total weight of other polymers.					

To clearly see DCB test result, graphs of each groups are plotted. Figure 4.7, Figure 4.8, Figure 4.9 and Figure 4.10 give load versus displacement graphs of each groups respectively. Table 4.3 summarizes calculated Mode I fracture toughness of produced composite laminates. Table 4.4 shows calculated percent change of G_{IC} values compared with Z1 reference composite and Z2 composite (only PA6 nanofibers interleaved composite laminate). The calculation of G_{IC} fracture toughness by using DCB test result is illustrated in Appendix C.

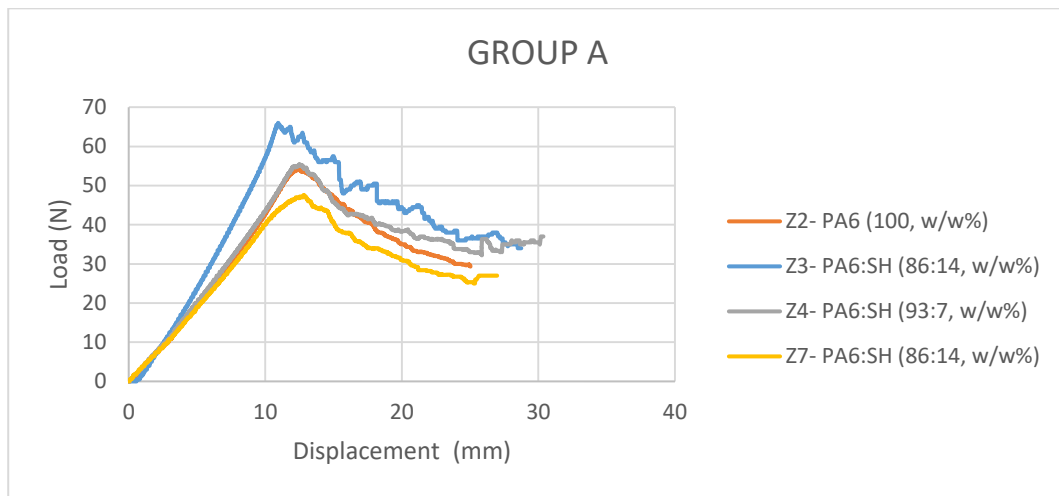


Figure 4.7 Plot of Group A composites in terms of load and displacement.

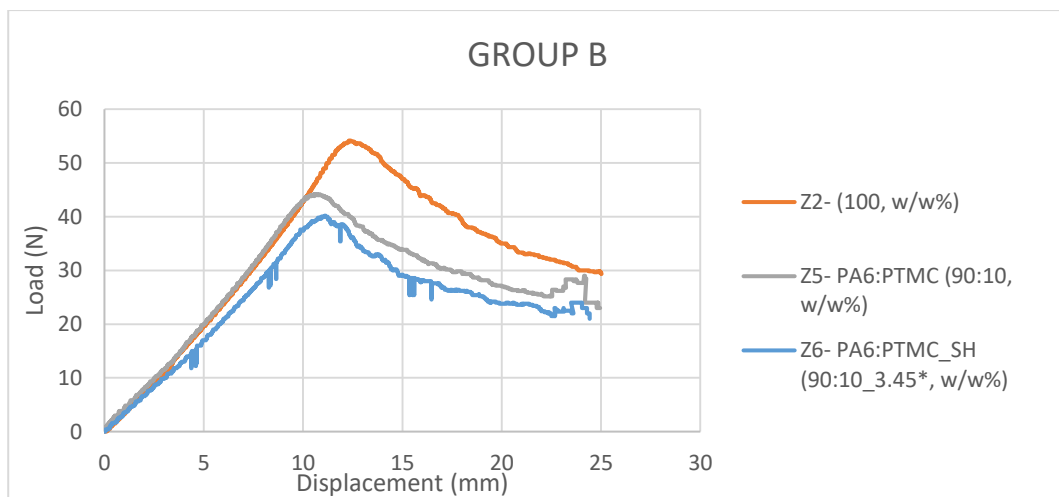


Figure 4.8 Plot of Group B composites in terms of load and displacement.

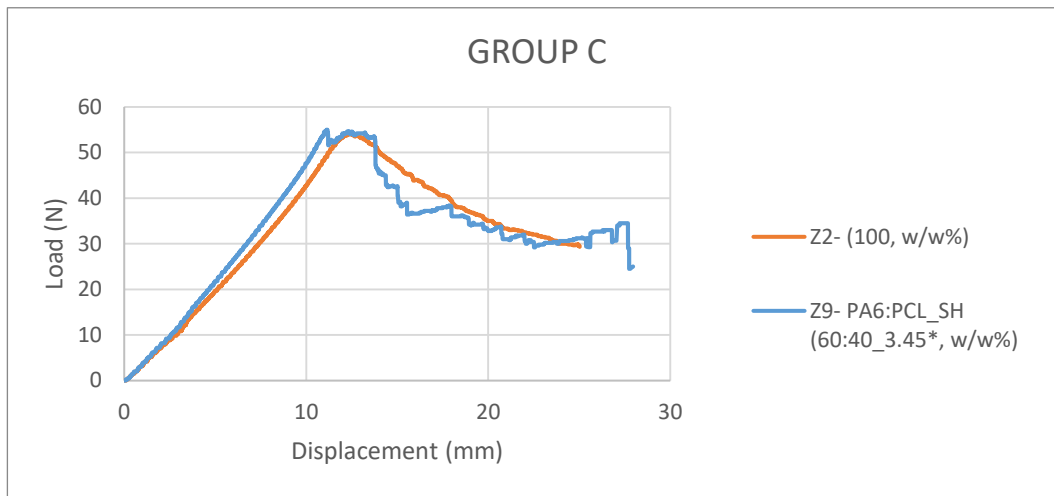


Figure 4.9 Plot of Group C composites in terms of load and displacement.

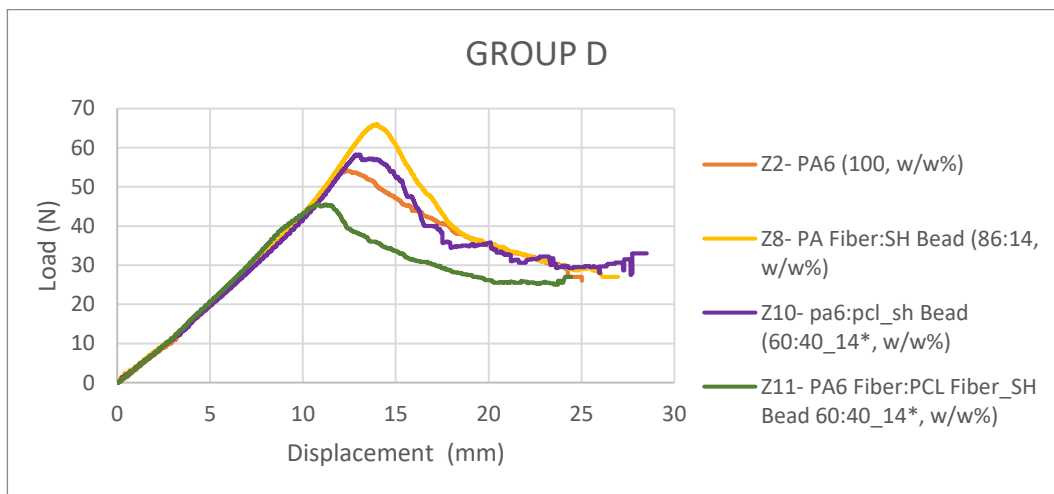


Figure 4.10 Plot of Group D composites in terms of load and displacement.

Table 4.3 DCB test results in terms of G_{IC} initiation and propagation values.

Sample	G_{IC} Initiation (J/m ²)	G_{IC} propagation (J/m ²)
Z1	750 ± 111	709 ± 147
Z2	586 ± 75	525 ± 65
Z3	702 ± 115	655 ± 47
Z4	564 ± 144	555 ± 130
Z5	393 ± 32	361 ± 50
Z6	397 ± 59	331 ± 47
Z7	482 ± 75	424 ± 52
Z8	847 ± 81	641 ± 46
Z9	569 ± 76	456 ± 106
Z10	647 ± 24	522 ± 51
Z11	424 ± 56	384 ± 53

Table 4.4 Percent change in G_{IC} initiation and propagation with respect to Z1 and Z2 laminates.

Sample	G_{IC} Initiation % change wrt Z1	G_{IC} Propagation % change wrt Z1	G_{IC} Initiation % change wrt Z2	G_{IC} Propagation % change wrt Z2
Z1	-	-	-	-
Z2	-22	-26	-	-
Z3	-6	-7	20	25
Z4	-25	-22	-4	+6
Z5	-48	-49	-33	-31
Z6	-47	-53	-32	-37
Z7	-36	-40	-18	-19
Z8	+13	-9	45	22
Z9	-24	-35	-3	-13
Z10	-14	-26	10	-0.5
Z11	-40	-46	-28	-27

At first glance, it is clearly seen from the graphs of load-displacement of each group that Z3 in Group A, Z2 in Group B and Group C, Z8 in Group D have a positive effect on displacement of crack growth. To obtain highest improvement among them, G_{IC} versus displacement curves of these three interleaved composite laminates and reference laminate were plotted in Figure 4.11.

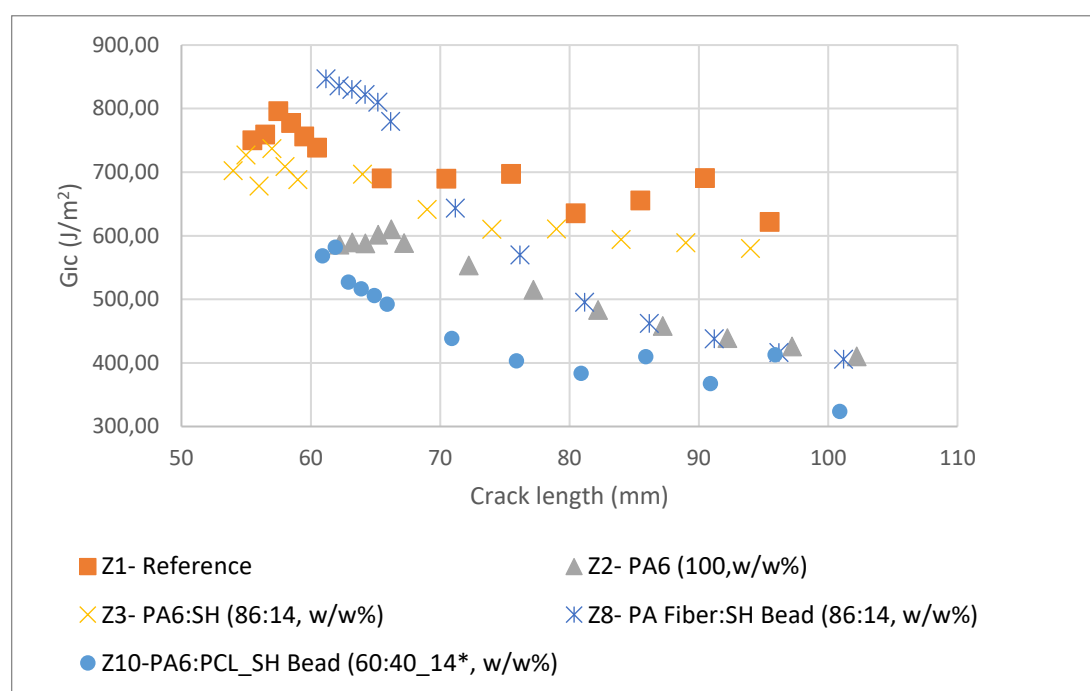


Figure 4.11 The plot of composites from each group which have greater improvement and reference in terms of G_{IC} and crack length..

According to Figure 4.11 and also Table 4.3, Z8 (PA6 nanofiber and shellac nanoparticles with 86:14 (w/w%) interleaved composite laminate) has greater improvement on G_{IC} compared to Z1 reference composite.

Moreover, Z3 which is interleaved with blends of PA6 and shellac nanofibers with beads composite laminate has G_{IC} initiation and propagation values compared to the Z2 (PA6 nanofiber interleaved composite laminate). Other interleaving attempts

generally led to a decrease in G_{IC} values. In order to understand effects of nanofibers interleaving on G_{IC} , fracture surfaces of tested specimens were characterized by SEM analysis. The interpretation of SEM micrographs of fracture surfaces of interphases was discussed in next section of this chapter, 4.4. Analysis of Fracture Surfaces.

4.4. Analysis of Fracture Surfaces

Fracture surfaces of tested DCB specimens were characterized by SEM analysis in order to verify the effect of nanointerleaving on composite laminates in terms of G_{IC} fracture toughness. The fracture interfaces of PA6 nanofiber interleaved composite laminate were shown in Figure 4.12. It is possible to see that nanofiber debonding and breakage shown with red arrows and circle. Nanofibers were deboned from epoxy matrix without exposing any deformation. Traces of debonding nanofibers (shown with blue arrow) were relatively smooth. This could be due to the weak interaction between PA6 and epoxy matrix. Therefore, they could not have any significant positive contribution to toughening mechanism because nanofibers could not wear to epoxy matrix then G_{IC} opening mode did not have any positive improvement. Moreover, in propagation stage of crack, there were some voids (indicated with yellow arrows) which indicate that heterogenous distribution of epoxy matrix. This void nucleation led to negative impact on fracture toughness because nanofibers could not find any holding area owing to epoxy poor areas.

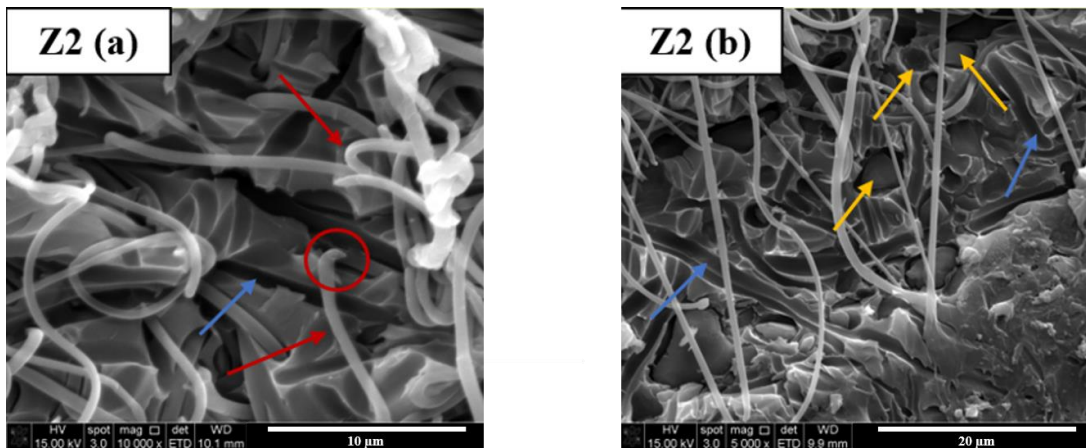


Figure 4.12 SEM micrograph of fracture surface of PA6 nanointerleaved composite laminate (Z2); (a) initiation, (b) propagation stage.

Z3 composite sample's fracture surface micrographs are illustrated in Figure 4.13. This composite was interleaved with nanofibers with beads veil produced by the blend of PA6 and shellac polymers with a weight ratio of 86% and 14% respectively. According to SEM analysis, it appears that shellac could make covalent bonding with epoxy matrix during the curing process of composite laminate. The expectation from hydroxyl and carboxyl groups of shellac is that they tend to react with epoxide group of epoxy resin. In the absence of hydroxyl group, etherification of epoxy ring takes place by means of ring opening reaction. And also, esterification of epoxy proceeds when carboxyl groups are present. As a consequence of all these reactions, crosslinked networks are achieved, and they make stronger media. It was seen in Figure 4.13, almost all nanofibers are embedded into epoxy matrix and some nanofibers were pulled-out with stretching (red circles and arrows). This helps to improve fracture toughness of laminate and increase G_{IC} . However, chemical bonding between shellac and epoxy creates highly strong but brittle interface; therefore, nanofibers could not be stretched during pull-out process and then break suddenly. This leads to sudden reduction in fracture toughness and limits the enhancement in G_{IC} . To solve this limitation, like PCL and PTMC elastomer thermoplastics were added to nanofiber system to contribute some flexibility to the matrix-nanofiber interface.

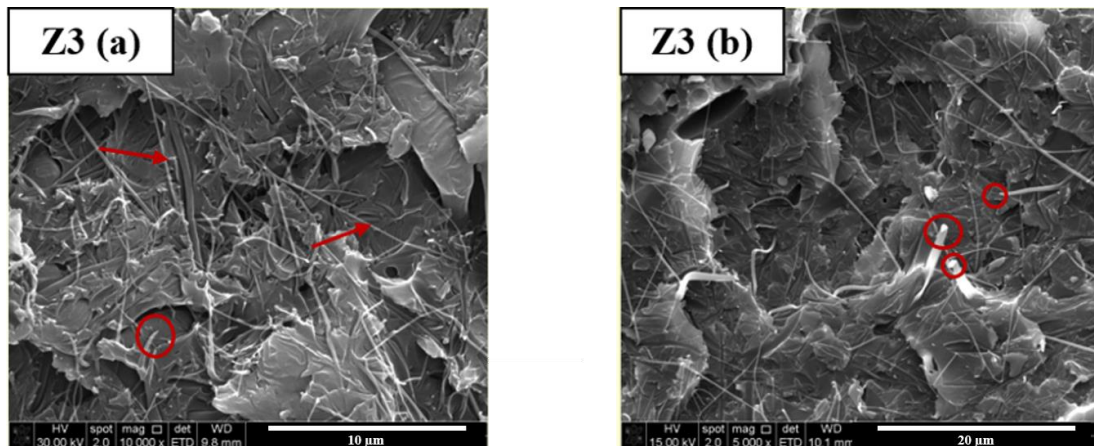


Figure 4.13 SEM micrograph of fracture surface of PA6 and shellac nanointerleaved composite laminate (Z3); (a) initiation, (b) propagation stage.

To decrease brittleness of interface of composite, the weight percent of shellac was decreased to 7% from 14% in total amount of polymer. In initiation stage of crack (Figure 4.14, (a)), only nanofiber debonding like in PA6 nanointerleaved composite was observed. However, in propagation stage of crack growth, green arrows indicate some bridging zones most probably created by interaction between shellac and epoxy. This helps to stretching nanofibers before pulling out. Therefore, G_{IC} value of Z4 composite has only little enhancement in propagation stages compared to G_{IC} propagation value of Z2 composite. We say that in this case, amount of shellac is not enough to make composite laminate interface stronger.

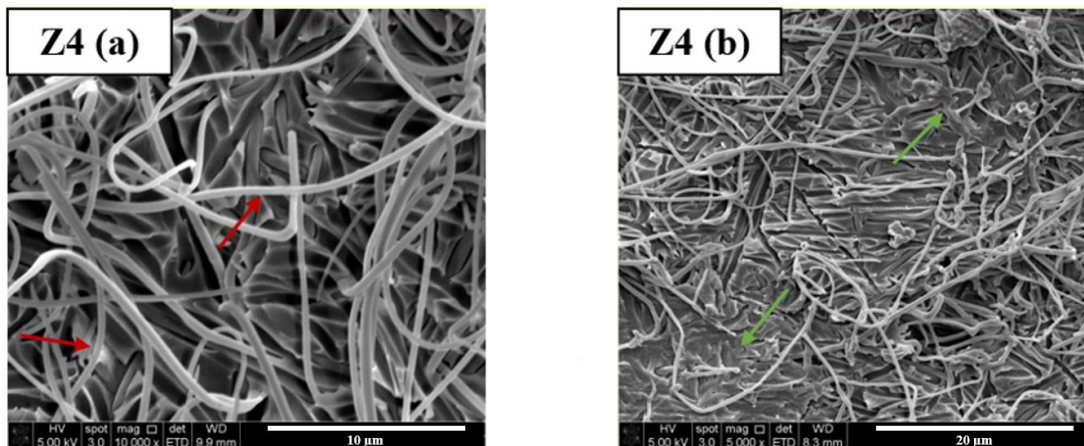


Figure 4.14 SEM micrograph of fracture surface of PA6 and shellac nanointerleaved composite laminate (Z4); (a) initiation, (b) propagation stage.

Elastomeric polymer could be an option for improving fiber elongation at break, but many elastomeric polymers have some difficulty in spinnability since they have low T_g viscosity and therefore, electrospun nanofibers turn into larger fibers or sometimes continuous film. To overcome this, elastomeric polymers could be used in blend with polymer which could be electropun very well [53]. In the light of this information, PTMC elastomeric polymer was chosen in order to blend with PA6. It could add some elasticity to interface and balance between matrix and nanofiber. To get influential toughening, intermediate interfacial strength should be advantageous since if it is too strong due to shellac and epoxy interaction, the result will be excessive debonding of nanofibers from matrix, thus decreases in G_{IC} mode. Figure 4.15 represents SEM micrographs of Z5 composite laminate which includes nanofibers mats consists of 90% PA6 and 10% PTMC by weight.

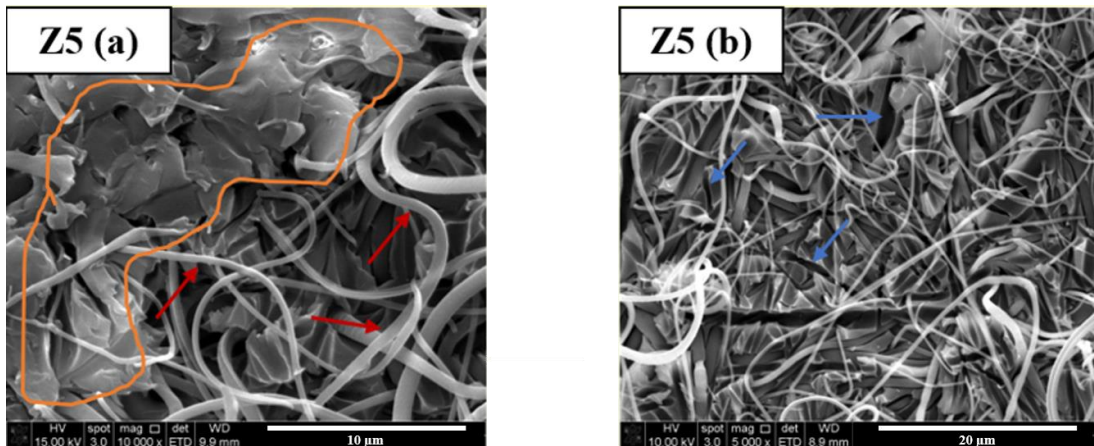


Figure 4.15 SEM micrograph of fracture surface of PA6 and PTMC nanointerleaved composite laminate (Z5); (a) initiation, (b) propagation stage.

By looking at the SEM images of fracture surface of Z5 composite, nanofibers mostly deboned from epoxy matrix (red arrows) and traces of debonding (blue arrows) indicated that there are some smooth pits which means no resistance during fiber debonding. Thus, there is a significant decrease in G_{IC} fracture toughness value (shown in Table 4.3). The aim of adding PTMC in the interface is that thanks to low T_g of elastomer, during curing process, PTMC dispersed into PA6 nanofibers and epoxy matrix and made a good adhesion in interface. Nevertheless, from the result, PTMC elastomer didn't meet our expectation and even has negative impact on G_{IC} values. The area with indicated orange line made of crowding PTMC polymer heterogeneously. Judicious number of nanofibers were peeled off phase-separated structure caused by PCL and epoxy resin. This led to weak adhesion between nanofibers and epoxy matrix and lower G_{IC}

Little amount of shellac was added to blend of PA6 and PTMC to strengthen interfacial toughening. Z6 composite laminate was produced with PA6, PTMC polymers (90 and 10 (w/w%) respectively) and 3.45 (w/w%) of total amount of polymer in fiber. It could be seen from Figure 4.16 that nanofibers mostly deboned in initiation without breaking in initiation crack growth. However, in propagation stage, nanofibers mainly embedded into epoxy matrix. This led to sudden fracture during

loading. Therefore, G_{IC} of Z6 composite laminate was reduced significantly compared to Z2 composite.

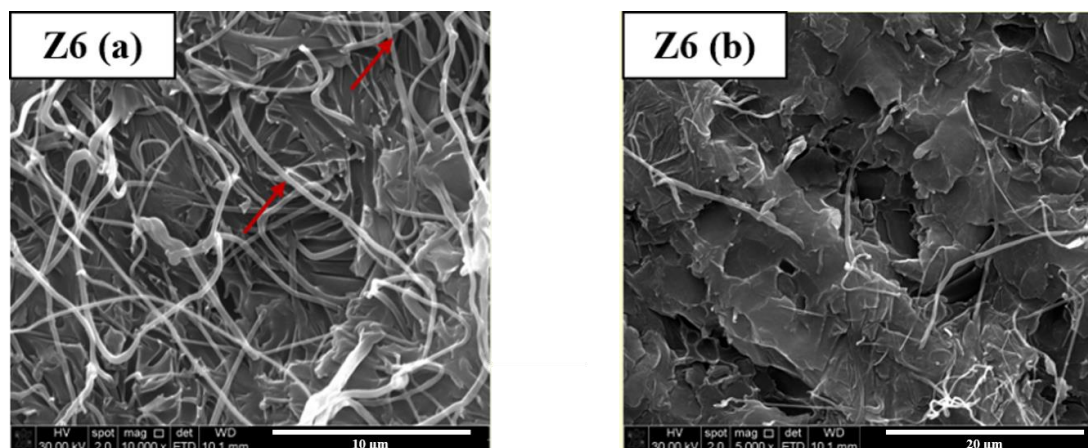


Figure 4.16 SEM micrograph of fracture surface of PA6, PTMC and shellac nanointerleaved composite laminate (Z6); (a) initiation, (b) propagation stage.

Results up to this point show that nanofibers with beads produced by the blend of PA6 and shellac improved G_{IC} fracture toughness (Z2). Therefore, nanofibers without beads configuration was studied to see the difference between these two nanofibers morphologies. As in Z3 interleaving mat, the same weight percentages of polymers were used in interleaving Z7 composite laminate. In order to produce beadless nanofiber morphology, the concentration of solution was increased in nanofibers for Z7 laminate.

G_{IC} result of Z7 interleaved composite laminate was lower than that of Z3 (see in Table 3.3). Fracture surface SEM images of Z7 (Figure 4.17) showed that extensive debonding occurred in initiation crack during DCB test. Whereas, in propagation crack growth, some nanofibers were embedded into epoxy matrix and some of them debonded and traces of their debonding was smooth. This proved that there is not much more resistance during debonding of nanofibers and resulted in lowering G_{IC} value. It could be inferred that beads have positive contribution to improvement in

interfacial strength and fracture toughness. Then, electrospaying over nanofibers was studied to observe contribution of nanoparticles in interfacial toughening.

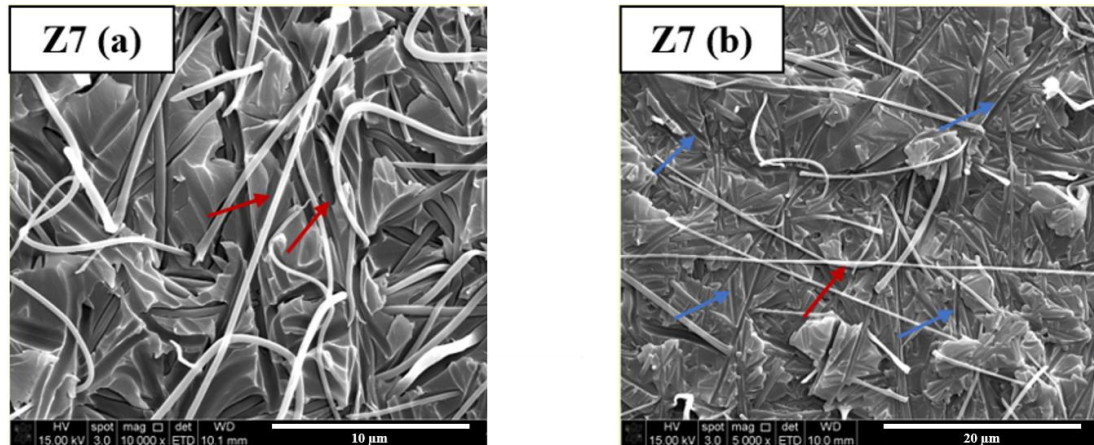


Figure 4.17 SEM micrograph of fracture surface of PA6 and shellac nanointerleaved composite laminate (Z7); (a) initiation, (b) propagation stage.

Z8 interleaved composite laminate was produced with nanofiber and nanoparticles mat which were produced by electrospinning and electrospaying. Again, the same weight percentage of PA6 and shellac polymers were used in interleaving layer as in Z3 and Z7 composite laminates. The difference in here was that shellac polymer was sprayed over PA6 nanofibers. The aim was that during curing process, shellac nanoparticles were melt and thanks to functional groups of shellac, it could form covalent bond with epoxy matrix and made some bridging zones in interface. This makes positive contribution to the resistance to fracture during impact loading. It is worth highlighting that surface area increases by adding PA6 nanofibrous interleaving veil and this might cause the formation of some plastic region on the crack tip. These plastic regions could absorb energy via crack pinning. It could be seen from SEM micrograph (Figure 4.18), in propagation stage, the surface of matrix was covered with nanofiber interleave mat and some nanofibers were blended with epoxy resin. Rupture of nanofibers in initiation stage micrograph (shown with red circles) was observed and

some of nanofibers were pulled-out epoxy matrix (red arrows). Red circles represent thinner and broken fibers which were occurred by stretching and partially stretching away from the matrix instead of completely deboned fibers. In propagation stage, white arrows show small islands which were probably formed by shellac and epoxy chemical bonding. These small islands were assumed to behave like bridging zones. They form spots in which PA6 nanofibers could be attached to epoxy matrix. Moreover, owing to this mechanism, fibers were strained without debonding and rupture under loading impact (shown with blue arrows). It could increase the pull-out mechanism of nanofibers. Via bridging, laminate absorbed more than the energy required for fracture. All these mechanisms like bridging zones, debonding and rupture of nanofibers mentioned for Z8 composite provide the highest enhancement in G_{IC} fracture toughness among all produced composite laminates during this study.

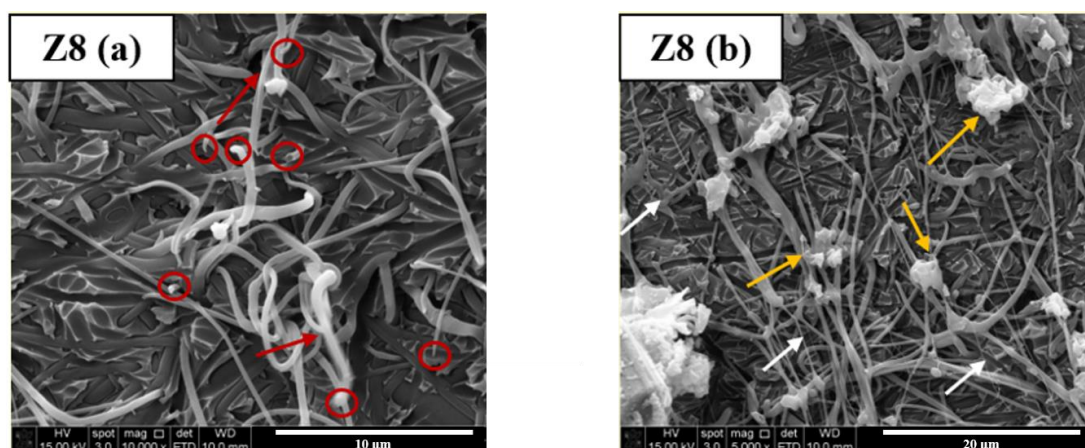


Figure 4.18 SEM micrograph of fracture surface of PA6 and shellac nanointerleaved composite laminate (Z8); (a) initiation, (b) propagation stage.

In order to get further improvement in G_{IC} , PCL was selected in addition to PA6 and shellac in production of nanofibers veil which was used in Z9. The role of PCL in there is to improve the adhesion between nanofibers and epoxy and add some elasticity for preventing excessive strength which was needed for good load transfer. PCL could easily dissolve during the curing process. With the diffusion of PCL into the holes

between PA6 nanofiber and epoxy, this adds positive contribution to peeling of PA6 nanofibers from matrix under loading. For production of Z9 nanofiber-interleaved composite, the percent amount of PA6 and PCL polymers were determined by means of previous study conducted by Kılıçoğlu [52] in 2018. According to this study [52], the best result was obtained with the nanofibers produced by the blends of PA6 and PCL whose weight percent in total polymer amount were 60 and 40 (w/w%) respectively. In addition, shellac with 3.45% of the total amount of polymer in fiber was added to enhance the adhesion of interface. Figure 4.19 shows fracture surface of nanofiber interleaved Z9 composite.

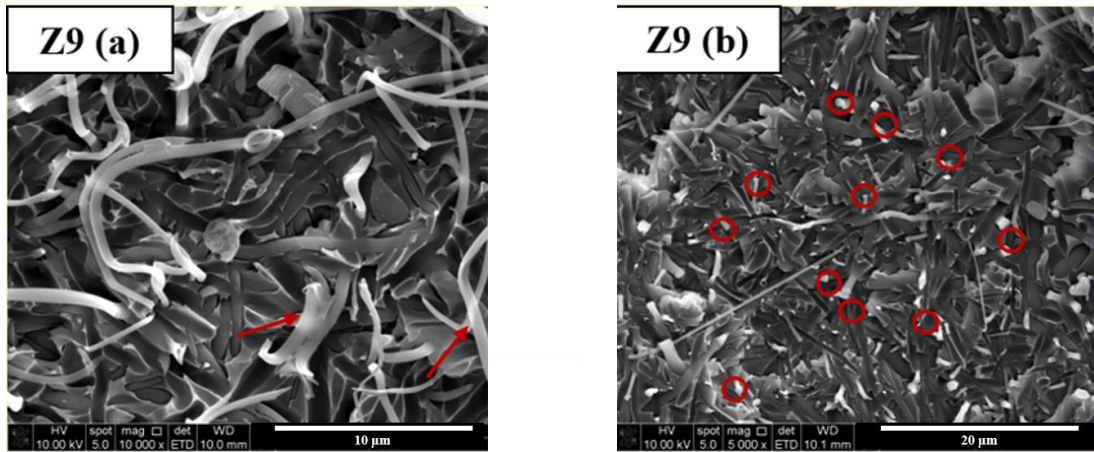


Figure 4.19 SEM micrograph of fracture surface of PA6, PCL and shellac nanointerleaved composite laminate (Z9); (a) initiation, (b) propagation stage.

SEM micrographs reveals that due to strong adhesion in interface, excessive peeling of nanofibers resulted in sudden breakage of nanofibers (see red circles). Then, it lowered G_{IC} fracture toughness.

Electrospraying of shellac was performed over nanofibers produced by the blend of PA6 and PCL whose weight percentages were the same as in Z9 interleaving mat for Z10 composite laminate. Shellac with 14% of total amount of polymer in fiber was sprayed over nanofiber mat. It could be seen from SEM images of Z10 fracture surface

(Figure 4.20) that some nanofibers were embedded into matrix and some of them were completely peeled from matrix. The imprints in fracture surface indicates lack of adhesion. Under impact, there was a decrease in G_{IC} fracture toughness because it was not enough energy absorption during loading.

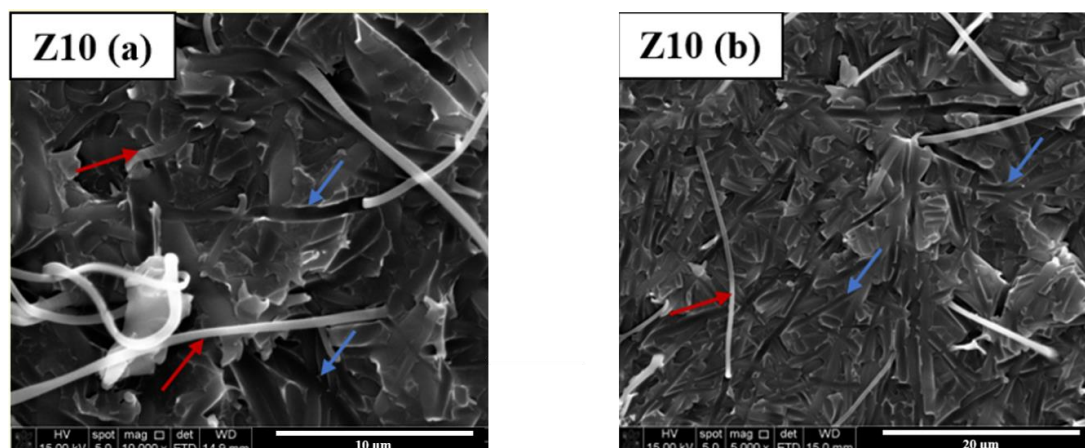


Figure 4.20 SEM micrograph of fracture surface of PA6, PCL and shellac nanointerleaved composite laminate (Z10); (a) initiation, (b) propagation stage.

For production of Z11 composite laminate, the same weight percentages of polymers were used as in Z10. Fracture interfaces shown in Figure 4.21 revealed that nanofibers did not have enough bridging zones which mainly resulted from chemical bonding of shellac and epoxy. Thus, most of nanofibers were deboned without much more deformation. G_{IC} fracture toughness was lower compared to PA6 nanofiber interleaved composite laminate (Z2).

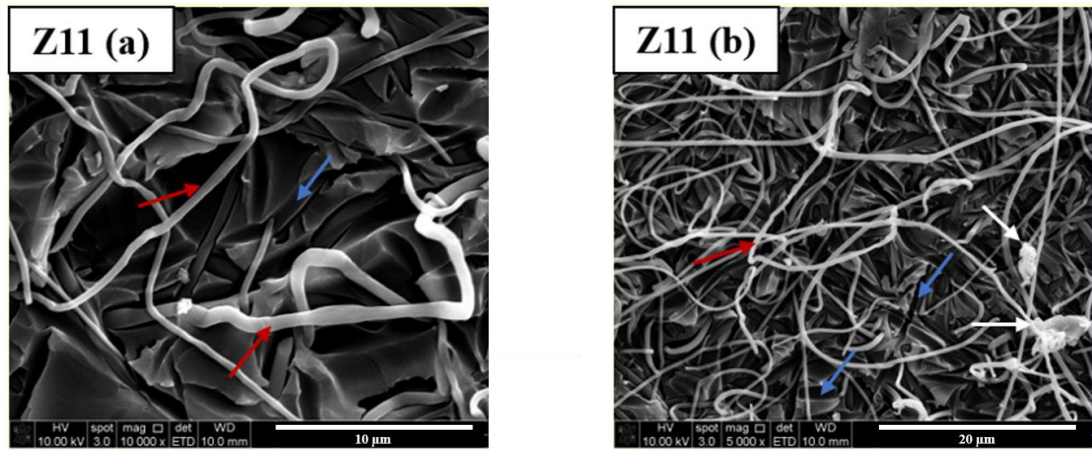


Figure 4.21 SEM micrograph of fracture surface of PA6, PCL and shellac nanointerleaved composite laminate (Z11); (a) initiation, (b) propagation stage.

CHAPTER 5

CONCLUSIONS

The aim of this study is to enhance G_{IC} fracture toughness value of composite laminates by nanofiber interleaving. PA6 nanofiber interleaved composite laminates have a great improvement on G_{IIC} delamination mode; whereas, it has no significant change or even reduction in G_{IC} value. G_{IC} fracture toughness has been affected from the adhesion between nanofibers and matrix. However, G_{IIC} does not affect this adhesion since shear adhesion is significant for G_{IIC} and this could be achieved with high surface area. Nanofibers have high surface area. Then, they improved shear adhesion and as a result, G_{IIC} value [54].

In this study, electrospinning technique was used for the production of interleaving nanofibers veils. Four different polymers (PA6, PTMC, PCL and shellac) were used during whole study. PA6 was the base polymer in nanofibers veil. In the first place, shellac was studied in nanofiber system by changing its amount of weight percent and concentration in the solution used in production for nano-interleaving veils. These composites are denoted in Group A. As a result of adding shellac to the interleaving system, an improvement on G_{IC} fracture toughness was achieved since interface of composite laminate is getting stronger by means of crosslinking caused by epoxy resin and shellac. From Group A, Z3 and Z7 composites were interleaved with nanoveils which were produced same amount of weight percent of polymer. The difference came from the concentration of polymeric solution used in production of nanofiber veils. Z3 is interleaved by veils composed of nanofibers with beads morphology. On the other hand, nanofiber veils of Z7 composite laminate was made from only smooth nanofiber morphology. Then, by comparing G_{IC} fracture toughness values of these two composites, nanofibers with beads morphology has greater impact on delamination. By the way, SEM micrographs of fracture surface of Group A composites also showed that besides shellac getting stronger the interface, it makes also brittle composite

laminate. Then, in order to decrease brittleness, PTMC was chosen as a third polymer in this system due to its elasticity. Group B is composed of composites produced for seeing the effects of PTMC in addition to that of shellac. However, with the addition of PTMC, and also PTMC plus shellac did not meet desired performance and lowered G_{IC} . Only PTMC addition caused heterogeneity and formed some space in matrix. Then, shellac addition in the PA6 and PTMC nanofiber system made stronger interface and resulted in sudden opening during DCB test according to SEM micrographs of fracture surface's related composites. PCL polymer decided to be used instead of PTMC because of same reasons such as low T_g value and elasticity. Group C is made up of composites produced by PCL and additionally shellac polymers used with PA6 in the interleaving veils. Before, PCL was worked with PA6 polymer in nano-interleaving veil system in Kılıçoğlu's study [52]. According to this study, nanofiber system which resulted in the highest improvement on G_{IC} fracture toughness was chosen and additionally shellac was added to this system to get more stronger composite interface owing to chemical bonding between functional groups of epoxy resin and shellac. On the other hand, there was a decrease in G_{IC} and to understand the reason for that SEM micrographs were analyzed. Then, excessive pulling of nanofibers due to embedded nanofibers in matrix was lowered toughness of composite laminate. The last one, Group D was designed by looking at the output from fiber morphologies in Group A. To get beads form, electrospaying process was studied alongside electrospinning for Group D composite laminates. In this group, shellac was electrospayed as beads over different nanofiber system. Sandwich structure was made up of PA6 nanofiber, PCL nanofiber and shellac beads. However, this interleaving did not form bridging zones in composite interface and excessive pulling of nanofibers caused decrease in G_{IC} fracture toughness. The highest enhancement on G_{IC} fracture toughness was achieved with veil consisting of PA6 nanofibers with shellac nanoparticles (Z8). Z8 has the same polymer weight percentage as in like Z3. The difference between Z3 and Z8 composites is that beads in Z8 composite laminate were produced by electrospaying technique.

To conclude, G_{IC} fracture toughness values were measured for all produced interleaved composite laminates. Among them, when compared with Z1 reference composite which has no interleaving material, veil consisting of PA6 nanofibers with shellac nanoparticles gave the highest enhancement which was the increase in G_{IC} by 13% in initiation stage of crack growth. On the other hand, when comparing with only PA6 nanofibers veil interleaved composite laminate (Z2), Z8 laminate has an enhancement in G_{IC} by 45% and 22% in initiation and propagation stage of crack growth respectively. Moreover, nanofibers with beads veil which was produced by the blend of PA6 and shellac resulted also an increment in G_{IC} fracture toughness value by 20% for initiation and 25% for propagation stage (Z3), again compared to only PA6 nanofibers interleaved composite laminate (Z2). Both Z3 and Z8 composites, in addition to nanofibers, beads form was observed. By looking at SEM fracture surface of composite laminates, these beads were made up of shellac. And, during curing process of composite, its functional groups form covalent bonding with that of epoxy resin. As a result, an increment observed in G_{IC} fracture toughness.

CHAPTER 6

RECOMMENDATIONS

In the light of this study, there are some suggestions that might be viable for improving this work. These are;

- In order to eliminate shellac spreading to environment due to the rotation of collector, shellac could be electrosprayed or electrospun directly over the surface of the prepreg by re-designing experimental setup.
- In order to get more reliable comparison of results, electrospinning might be performed directly over the surface of prepreg. In this way, loss due to transferring nanofibers veil on the prepreg could be minimized.
- Crosslinking of PTMC elastomeric polymer could be studied in order to create good adhesion with epoxy matrix.
- Other crosslinkable elastomeric polymers might be studied with PA6 in nanofibers system.
- G_{IC} values of each composites might be measured in order to see the effect of nanointerleaving on shearing.

REFERENCES

- [1] W. G. Roeseler, B. Sarh, and M. U. Kismarton, "Composite Structures: the First 100 Years," 2007, pp. 1–10.
- [2] M. Mrazova, "Advanced composite materials of the future in aerospace industry," vol. 5, no. 3, pp. 139–150, 2013.
- [3] L. Daelemans, S. Van Der Heijden, I. De Baere, H. Rahier, W. Van Paepegem, and K. De Clerck, "Damage-Resistant Composites Using Electrospun Nano fibers : A Multiscale Analysis of the Toughening Mechanisms," *Appl. Mater.*, vol. 8, pp. 11806–11818, 2016.
- [4] A.-H. M. R. Ziadoon and Z. Chwei, "Effect the stacking sequences of composite laminates under low velocity impact on failure modes by using carbon fiber reinforced polymer," *Int. J. Eng. Sci. //*, vol. 5, no. 2, pp. 53–62, 2016.
- [5] H. Saghafi, A. Zucchelli, R. Palazzetti, and G. Minak, "The effect of interleaved composite nanofibrous mats on delamination behavior of polymeric composite materials," *Compos. Struct.*, vol. 109, pp. 41–47, 2014.
- [6] G. W. Beckermann and K. L. Pickering, "Mode I and Mode II interlaminar fracture toughness of composite laminates interleaved with electrospun nanofibre veils," *Compos. Part A Appl. Sci. Manuf.*, vol. 72, pp. 11–21, 2015.
- [7] H. Saghafi, R. Palazzetti, A. Zucchelli, and G. Minak, "Influence of electrospun nanofibers on the interlaminar properties of unidirectional epoxy resin / glass fiber composite laminates," *J. Reinf. Plast.*, 2015.
- [8] R. Palazzetti, X. Yan, and A. Zucchelli, "Influence of Geometrical Features of Electrospun Nylon 6 , 6 Interleave on the CFRP Laminates Mechanical Properties," *Polym. Compos.*, 2014.
- [9] B. De Schoenmaker, S. Van Der Heijden, I. De Baere, W. Van, and K. De Clerck, "Effect of electrospun polyamide 6 nanofibres on the mechanical properties of a glass fibre/epoxy composite," vol. 32, pp. 1495–1501, 2013.
- [10] S. Yilmaz, O. Gul, and T. Yilmaz, "Effect of chain extender and terpolymers on tensile and fracture properties of polyamide 6," *Polymer (Guildf)*., vol. 65, p. 8900, 2015.
- [11] A. Dhawale, "Shellac for Film Formation and Its Modification for Enhancement of Properties," vol. 64, pp. 1–8, 2014.

- [12] “Composites”, 2013. [Online]. Available: <http://www.essentialchemicalindustry.org/materials-and-applications/composites.html>. [Accessed: 25-Aug-2018].
- [13] G. Staab, *Laminar Composites*, 2nd ed. Elsevier Ltd, 2015.
- [14] N. Godin, P. Reynaud, and G. Fantozzi, “Contribution of AE analysis in order to evaluate time to failure of ceramic matrix composites,” *Eng. Fract. Mech.*, vol. 210, pp. 452–469, 2019.
- [15] E. Salur, A. Aslan, M. Kuntoglu, A. Gunes, and O. Sinan, “Experimental study and analysis of machinability characteristics of metal matrix composites during drilling,” *Compos. Part B*, vol. 166, pp. 401–413, 2019.
- [16] C. Elanchezhian, B. V. Ramnath, G. Ramakrishnan, K. N. S. Raghavendra, M. Muralidharan, and V. Kishore, “Review on metal matrix composites for marine applications,” *Mater. Today Proc.*, vol. 5, pp. 1211–1218, 2018.
- [17] D. D. L. Chung, “A review of multifunctional polymer-matrix structural composites,” *Compos. Part B*, vol. 160, pp. 644–660, 2019.
- [18] E. Fitzer, A. Gkogkidis, and M. Heine, “Carbon fibres and their composites,” *High Temp. Press.*, vol. 16, pp. 363–392, 1984.
- [19] N. Forintos and T. Czigany, “Multifunctional application of carbon fiber reinforced polymer composites : Electrical properties of the reinforcing carbon fibers – A short review,” *Compos. Part B*, vol. 162, pp. 331–343, 2019.
- [20] J. M. Stickel and M. Nagarajan, “Glass Fiber-Reinforced Composites : From Formulation to Application,” *Intern. J. Appl. Glas. Sci.*, vol. 136, pp. 122–136, 2012.
- [21] S. Mazumdar, *Composites Manufacturing Materials, Product and Process Engineering*. CRC Press, 2001.
- [22] M. S. Kırgız, “Green cement composite concept reinforced by graphite nano-engineered particle suspension for infrastructure renewal material,” *Compos. Part B Eng.*, vol. 154, pp. 423–429, 2018.
- [23] J. R. Kelly, H. Wellesley, and Mass, “Dispersion Strengthened Composite,” 1990.
- [24] A. G. Mamalis, D. E. Manolacos, M. B. Ioannidis, and D. P. Papapostolou, “On the crushing response of composite sandwich panels subjected to edgewise compression: Experimental,” *Compos. Struct.*, vol. 71, pp. 246–257, 2005.
- [25] R. P. L. Nijssen, *Composite Materials: An Introduction*. 2015.
- [26] N. Taniguchi, T. Nishiwaki, and H. Kawada, “Tensile strength of unidirectional CFRP laminate under high strain rate,” *Adv. Compos. Mater. Off. J. Japan Soc. Compos. Mater.*, vol. 16, no. 2, pp. 167–180, 2007.

- [27] G. P. Thomas, “Composite Prepregs- Manufacturing, Benefits and Applications,” 2013. [Online]. Available: <https://www.azom.com/article.aspx?ArticleID=8353>.
- [28] F. C. Campbell, “Introduction to Composite Materials,” 2010, p. 630.
- [29] J. N. Reddy and A. Miravete, *Practical Analysis of Composite Laminates*. CRP Press, 1995.
- [30] “Pre-consolidated, multiaxial, thermoplastic composite structures,” 2014. [Online]. Available: <https://www.compositesworld.com/products/pre-consolidated-multiaxial-thermoplastic-composite-structures>.
- [31] Q.-Q. Ni, J. Xie, and Z. Maekawa, “Buckling Analysis of Laminated Composite Plates Using Higher-Order Shear Deformation Theory.”
- [32] “Damage Mechanisms in Unidirectional Composites.” [Online]. Available: https://nptel.ac.in/courses/101104010/lecture20/20_7.htm.
- [33] R. H. Martin, “Evaluation of the Split Cantilever Beam for Mode III Testing,” *ASTM STP*, vol. 1110, pp. 243–266, 1991.
- [34] S. L. Donaldson, S. Mall, and C. Lingg, “The Split Cantilever Beam Test for Characterizing Mode III Interlaminar Fracture Toughness,” *JCTRE*, vol. 13, pp. 41–47, 1991.
- [35] J. Verrey, Y. Winkler, V. Michaud, and J. A. E. Månson, “Interlaminar fracture toughness improvement in composites with hyperbranched polymer modified resin,” *Compos. Sci. Technol.*, vol. 65, no. 10, pp. 1527–1536, 2005.
- [36] P. K. Mallick, *Composites Engineering Handbook*. CRC Press, 1997.
- [37] W. E. Howard, T. G. Jr., and R. M. Jones, “Composite Laminate Free-Edge Reinforcement with U-Shaped Caps Part I: Stress Analysis,” *AIAA J.*, vol. 27, no. 5, pp. 617–623, 1989.
- [38] L. A. Mignery, T. M. Tan, and C. T. Sun, “The use of stitching to suppress delamination in laminated composites,” *Delamination Debonding Mater.*, vol. 876, pp. 371–385, 1985.
- [39] M. Hojo, S. Matsuda, M. Tanaka, S. Ochiai, and A. Murakami, “Mode I delamination fatigue properties of interlayer-toughened CF / epoxy laminates,” *Compos. Sci. Technol.*, vol. 66, pp. 665–675, 2006.
- [40] K. Shivakumar *et al.*, “Polymer Nanofabric Interleaved Composite Laminates,” in *Structures, Structural Dynamics, and Materials Conference*, 2009, no. May.
- [41] G. T. Kim *et al.*, “Effect of Humidity on the Microstructures of Electrospun Polystyrene Nanofibers,” *Microsc. Soc. Am.*, pp. 554–555, 2004.

- [42] C. Mit-uppatham, M. Nithitanakul, and P. Supaphol, "Ultrafine Electrospun Polyamide-6 Fibers : Effect of Solution Conditions on Morphology and Average Fiber Diameter," vol. 6, pp. 2327–2338, 2004.
- [43] K. H. Lee, H. Y. Kim, M. S. Khil, Y. M. Ra, and D. R. Lee, "Characterization of nano-structured poly(E-caprolactone) nonwoven mats via electrospinning," vol. 44, pp. 1287–1294, 2003.
- [44] A. A. Almetwally, M. El-Sakhawy, M. H. Elshakankery, and M. H. Kasem, "Technology of Nano-Fibers : Production Techniques and Properties - Critical Review," 2017.
- [45] M. G. McKee, G. L. Wilkes, R. H. Colby, and T. E. Long, "Correlations of Solution Rheology with Electrospun Fiber Formation of Linear and Branched Polyesters," *Macromolecules*, vol. 37, pp. 1760–1767, 2004.
- [46] C. S. Ki, D. H. Baek, K. D. Gang, K. H. Lee, I. C. Um, and Y. H. Park, "Characterization of gelatin nanofiber prepared from gelatin-formic acid solution," *Polymer (Guildf.)*, vol. 46, pp. 5094–5102, 2005.
- [47] S. Megelski, J. S. Stephens, D. B. Chase, and J. F. Rabolt, "Micro- and Nanostructured Surface Morphology on Electrospun Polymer Fibers," *Macromolecules*, vol. 35, pp. 8456–8466, 2002.
- [48] G. Li *et al.*, "Novel carbon fiber / epoxy composite toughened by electrospun polysulfone nanofibers," *Mater. Lett.*, vol. 62, pp. 511–514, 2008.
- [49] H. Saghafi, T. Brugo, G. Minak, and A. Zucchelli, "The effect of PVDF nanofibers on mode-I fracture toughness of composite materials," *Compos. Part B*, vol. 72, pp. 213–216, 2015.
- [50] N. Tien, M. H. Gabr, K. Okubo, B. Chuong, and T. Fujii, "Improvement in the mechanical performances of carbon fiber / epoxy composite with addition of nano- (Polyvinyl alcohol) fibers," *Compos. Struct.*, vol. 99, pp. 380–387, 2013.
- [51] J. Zhang, T. Yang, T. Lin, and C. H. Wang, "Phase morphology of nanofibre interlayers : Critical factor for toughening carbon / epoxy composites," *Compos. Sci. Technol.*, vol. 72, pp. 256–262, 2012.
- [52] M. Kılıçoğlu, "Nano-Melez Sistemlerin Karbon Fiber Takviyeli Polimer Matris Kompozitlerde (KFTP) Arayüz Toklaştırma Amacıyla Kullanımı," Hacettepe University, 2018.
- [53] F. Jian, T. Lin, W. Tian, A. Sharma, and X. Wang, "Toughened Electrospun Nanofibers from Crosslinked Elastomer-Thermoplastic Blends," *J. Appl. Polym. Sci.*, vol. 105, pp. 2321–2326, 2007.
- [54] J. F. Najem, S. C. Wong, and G. Ji, "Shear adhesion strength of aligned electrospun nanofibers," *Langmuir*, vol. 30, pp. 10410–10418, 2014.

- [55] ASTM International, “D5528-01: Standard Test Method for Mode I Interlaminar Fracture Toughness of Unidirectional Fiber-Reinforced Polymer Matrix Composites 1,” *Am. Stand. Test. Methods*, vol. 03, no. Reapproved 2007, pp. 1–12, 2014.

APPENDICES

A. Gel Permeation Chromatogram of Synthesized PTMC

GPC chromatogram of PTMC with Mw of 53,090 g/mol is given in Figure A 1.

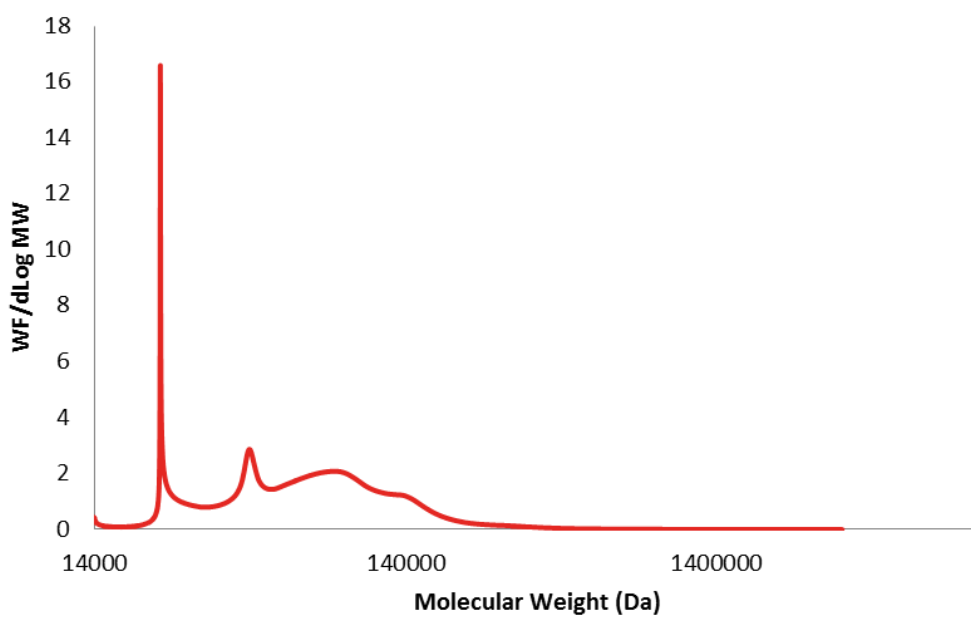


Figure A 1 Chromatogram of synthesized two-armed PTMC.

B. The Contents of Electrospinning and Electro spraying Solutions

The contents of each electrospinning and electro spraying solutions are listed in Table B1.

Table B 1 Ingredients of electrospinning and electro spraying solutions.

ES-1	PA6 (%w)			
	100			
	PA6 (g)	TFE (PA6) mL	PA6 %	PA6 % in ES
	1.206	6.4	12.06820638	12.06820638
ES-2	PA6 (%w)	Shellac (%w)		
	86	14		
	PA6 (g)	TFE (PA6) mL	PA6 %	PA6 % in ES
	1	7	9.424182452	6.148170919
	Shellac (g)	TFE (Sh) mL	Shellac %	Shellac % in ES
	0.162	4	2.865228157	0.996003689
ES-3	PA6 (%w)	Shellac (%w)		
	93.02325581	6.976744186		
	PA6 (g)	TFE (PA6) mL	PA6 %	PA6 % in ES
	1.4	7	12.71455817	10.6257827
	Shellac (g)	TFE (Sh) mL	Shellac %	Shellac % in ES
	0.105	1.5	4.851004851	0.796933703
ES-4	PA6 (%w)	PTMC (%w)		
	89.89574091	10.10425909		
	PA6 (g)	TFE (PA6) mL	PA6 %	PA6 % in ES
	1.621	8.4	12.32306032	9.286524514
	PTMC (g)	TFE (PTMC) mL	PTMC %	PTMC % in ES
	0.1822	3	4.236027155	1.043803064

ES-5	PA6 (%w) 89.89803835	PTMC (%w) 10.10196165		
	PA6 (g) 1.6223	TFE (PA6) mL 8.4	PA6 % 12.33172437	PA6 % in ES 8.285114576
	PTMC (g) 0.1823	TFE (PTMC) mL 3	PTMC % 4.238253551	PTMC % in ES 0.9310093
	Shellac (g) 0.0646	TFE (Sh) mL 1.5	Shellac % 3.041288075	Shellac % in ES 0.329913334
ES-6	PA6 (%w) 86.05851979	Shellac (%w) 13.94148021		
	PA6 (g) 1	TFE (PA6) mL 4	PA6 % 15.40357363	PA6 % in ES 10.63829787
	Shellac (g) 0.162	TFE (Sh) mL 2	Shellac % 5.570839065	Shellac % in ES 1.723404255
ES-7	PA6 (%w) 86	Shellac (%w) 14		
	PA6 (g) 1	TFE (PA6) mL 6	PA6 % 10.82485386	
	Shellac (g) 1.5	EtOH (Sh) mL 6	Shellac % 24.06159769	
ES-8	PA6 (%w) 59.99872098	PCL (%w) 40.00127902		
	PA6 (g) 0.9382	TFE (PA6) mL 4.8	PA6 % 12.46181229	PA6 % in ES 5.475694384
	PCL (g) 0.6255	TFE (PCL) mL 5.5	PCL % 7.649504708	PCL % in ES 3.650657469
	Shellac (g) 0.0553	TFE (Sh) mL 1	Shellac % 3.87173563	Shellac % in ES 0.322751971

ES-9	PA6 (%w) 59.99872098	PCL (%w) 40.00127902		
	PA6 (g) 0.9382	TFE (PA6) mL 4.8	PA6 % 12.46181229	PA6 % in ES 5.973665444
	PCL (g) 0.6255	TFE (PCL) mL 5.5	PCL % 7.649504708	PCL % in ES 3.982655868
	Shellac (g) 3	EtOH (Sh) mL 9	Shellac % 29.7000297	
ES-10	PA6 (%w) 60	PCL (%w) 40		
	PA6 (g) 1.0025	TFE (PA6) mL 6	PA6 % 10.84898003	
	PCL (g) 1.0064	TFE (PCL) mL 6	PCL % 10.8865908	
	Shellac (g) 1.0093	EtOH (Sh) mL 7.2	Shellac % 15.08647105	

C. Example for Calculation of G_{IC} According to ASTM-D5528

In this work, 6 specimens were tested for calculation G_{IC} from DCB test results. DCB test machine which was used during this study is shown in Figure C 1.

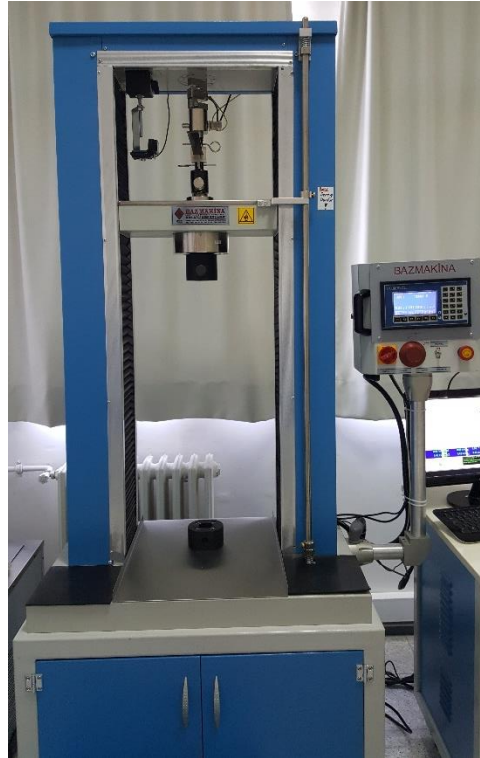


Figure C 1 DCB test machine.

After fixing heads, the distance between fixing heads and the initial point of Teflon tape was measured by means of calipers and recorded as “ a_{teflon} ” value. Then, test sample was placed in DCB tester and, loading (Figure C 2) as well as test was started.



Figure C 2 Test specimen under loading.

When crack was proceeded, load and displacement values for every marked point were recorded by manually. Figure C 3 illustrates crack growth along the test specimen.



Figure C 3 Crack growth along the specimen under loading.

When the crack was reached to 45 mm and for each point, load and displacement values were recorded, the graph of load versus displacement and recorded values were written as in shown in Figure C 4.

The screenshot shows a software window titled "Tablo Kamera" with a table of data. The table has the following columns: a (mm), P (N), d (mm), and t (mm). The rows are numbered 1 to 18. A green button labeled "Veri Al" is positioned to the left of the table. Below the table is a button labeled "Hesapla".

		a (mm)	P (N)	d (mm)	t (mm)
1	a teflon	57.5	82	12.6364392	
2	a pre-crack	5	78	14.2632292	
3	a0 VIS	5	71	14.148266	
4	a1	6	71	14.1747804	
5	a2	7	71	14.7339104	
6	a3	8	68	15.0764724	
7	a4	9	68	15.1392164	
8	a5	10	62	15.6421804	
9	a6	15	50	16.7422244	
10	a7	20	45	17.2152332	
11	a8	25	39	18.2171132	
12	a9	30	36	20.2011392	
13	a10	35	33	22.0381216	
14	a11	40	31	23.8425176	
15	a12	45	28	25.902646	
16	a13				
17	a14				
18	a15				

Figure C 4 Measured crack length and load values by DCB.

Crack length (a), load (P) and displacement (d) values written in the right hand-side of Figure C 4 transferred to excel in order to calculate exact G_{IC} fracture toughness values (Figure C 5).

	A	B	C	D	E	F	G	H	I	J	K	L	M	N
1			a(mm)	P(N)	d(mm)	(s)	G(J/m ²)			C ^{1/3}	a(m)	a(mm)		G
2														
3	1	a teflon	55.8	57	9.7213732	530.11		0		0	0	0		
4	2	a pre-cra	5	63	12.7232688	693.53	760.6	0		0	0	0		757.8965
5	3	a0 VIS	5	59	12.7310612	694.09	712.74	0.215781		0.599797	0.0608	60.8		710.2108
6	4	a1	6	59	12.7756904	696.36	703.66	0.216537		0.600497	0.0618	61.8		701.2084
7	5	a2	7	59	13.1113708	714.71	710.65	0.222227		0.605711	0.0628	62.8		708.2128
8	6	a3	8	59	13.4968416	735.85	720.08	0.22876		0.61159	0.0638	63.8		717.6459
9	7	a4	9	58	13.8784668	756.52	716.66	0.239284		0.620828	0.0648	64.8		714.2724
10	8	a5	10	55	14.338016	781.95	691.42	0.260691		0.638816	0.0658	65.8		689.1555
11	9	a6	15	46	15.198216	828.79	569.69	0.330396		0.691319	0.0708	70.8		567.9487
12	10	a7	20	40	16.2070788	883.7	493.42	0.405177		0.739971	0.0758	75.8		492.011
13	11	a8	25	36	17.705952	965.41	455.12	0.491832		0.789355	0.0808	80.8		453.9063
14	12	a9	30	33	18.854066	1028.02	418.36	0.571335		0.829781	0.0858	85.8		417.3065
15	13	a10	35	30	21.1874344	1155.42	403.86	0.706248		0.890538	0.0908	90.8		402.9002
16	14	a11	40	28	22.8493408	1245.66	385.29	0.816048		0.934484	0.0958	95.8		384.418
17	15	a12	45	27	24.6641604	1345.12	381.14	0.913487		0.970288	0.1008	100.8		380.3257

Figure C 5 Transfer measured values to Excel in order to calculate fracture toughness.

According to ASTM D5528[55], Modified Beam Theory (MBT) method is used to calculate G_{IC} . Firstly, overestimate GI value is calculated according to Equation-2 below.

Equation-2;

$$GI = \frac{3P\delta}{2ba}$$

Where;

P = Load

δ = Load point displacement

b= Specimen width

a= Delamination length

This GI value is overestimate since there may be a rotation caused by nonproper built-in of beam. To fix this rotation, $a + |\Delta|$ is used as delamination length. Then, the equation is revised to Equation-3 shown in below.

Equation-3;

$$GI = \frac{3P\delta}{2b(a + |\Delta|)}$$

Δ could be obtained experimentally with using the approach shown in Figure C 6.

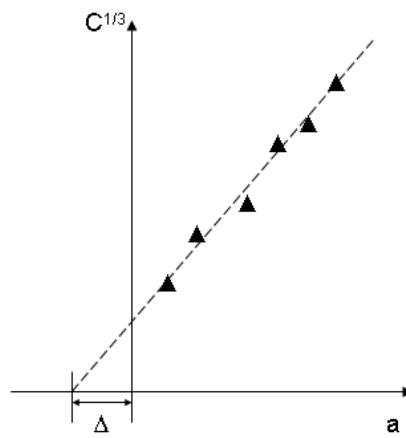


Figure C 6 Correction factor in Modified Beam Theory.

C is the compliance and calculated by δ/P (the ratio of load point displacement to applied load). The effective delamination extension, Δ , is obtained from the graph of the cube root of compliance versus delamination length. Figure C 7 represents how to calculate Δ from the plot of $C^{1/3}$ vs a . When $C^{1/3}$ is equal to zero the value on the x-axis is equal to Δ .

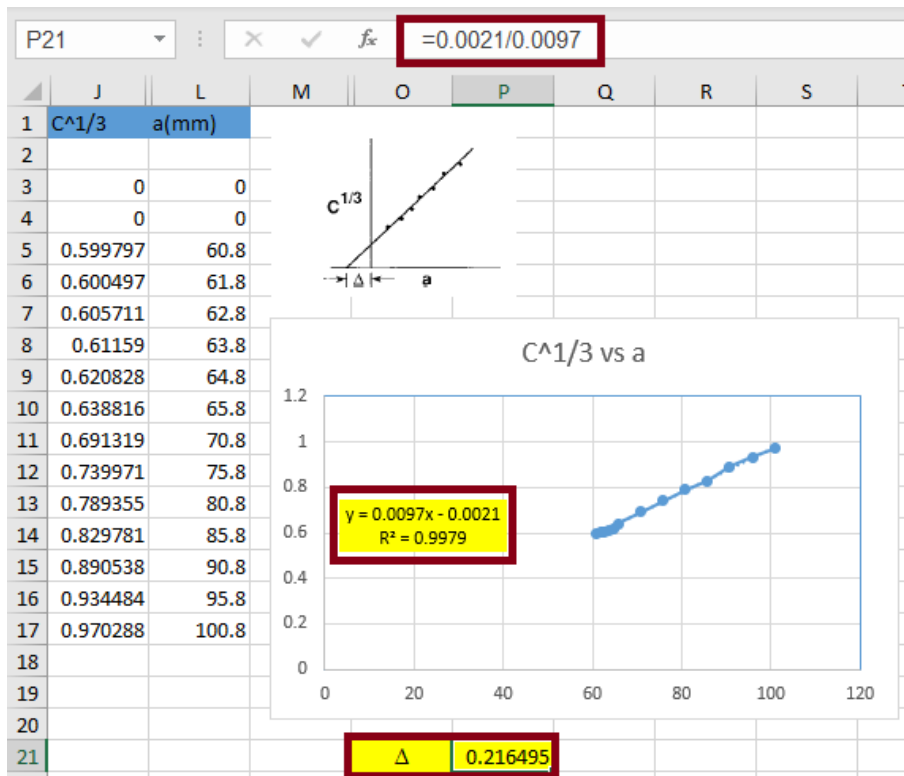


Figure C 7 Calculation of Δ .

Then, via Equation-3, G_{IC} values for each specimen are calculated. The graph of G_{IC} and a (mm) is plotted for each sample. Standard deviations are also calculated (in Figure C 8, column N and P) and added to graphs.

	A	B	C	D	E	F	G	H	I	J	K	L	M	N	O	P	
1	GIC (N/m)															crack size	
2	a1	T1	a2	T2	a3	T3	a4	T4	a5	T5	a6	T6	avg.	s.d.	avg.	s.d.	
3	60.8	710.2108	62.8	802.21	62.5	874.1635	60	893.5743	60.5	859.99	60.5	942.624	847.13	81.16347	61.2	1.168617	
4	61.8	701.2084	63.8	791.40	63.5	862.7876	61	880.923	61.5	848.61	61.5	932.1984	836.19	80.38277	62.2	1.168617	
5	62.8	687.6703	64.8	781.60	64.5	883.6892	62	869.1271	62.5	837.89	62.5	922.4327	830.40	84.40281	63.2	1.168617	
6	63.8	717.6459	65.8	785.29	65.5	853.5302	63	858.6288	63.5	826.41	63.5	892.5584	822.34	62.56228	64.2	1.168617	
7	64.8	714.2724	66.8	773.46	66.5	844.8899	64	847.9919	64.5	816.08	64.5	863.6856	810.06	56.70722	65.2	1.168617	
8	65.8	689.1555	67.8	756.45	67.5	784.7697	65	834.3346	65.5	808.16	65.5	808.0434	780.15	51.69447	66.2	1.168617	
9	70.8	567.9487	72.8	635.87	72.5	632.9943	70	704.1349	70.5	697.73	70.5	622.7263	643.57	50.84307	71.2	1.168617	
10	75.8	492.011	77.8	550.19	77.5	549.7618	75	623.9141	75.5	622.04	75.5	582.5278	570.07	50.31129	76.2	1.168617	
11	80.8	453.9063	82.8	492.96	82.5	474.9762	80	525.1969	80.5	528.26	80.5	498.3398	495.61	28.7091	81.2	1.168617	
12	85.8	417.3065	87.8	468.56	87.5	459.5628	85	502.065	85.5	463.34	85.5	461.9203	462.13	27.03089	86.2	1.168617	
13	90.8	402.9002	92.8	442.30	92.5	435.711	90	463.9469	90.5	451.37	90.5	433.4855	438.29	20.62828	91.2	1.168617	
14	95.8	384.418	97.8	418.54	97.5	420.959	95	440.2821	95.5	421.02	95.5	413.4128	416.44	18.1595	96.2	1.168617	
15	100.8	380.3257	102.8	416.43	102.5	393.6439	100	426.9263	100.5	413.90	100.5	404.1684	405.90	16.87833	101.2	1.168617	
16	avg.	550.73		624.25		651.65		682.39		661.14		675.24	640.90	45.6925			
17	s.d.	143.79		162.21		201.87		189.99		182.87		221.29	183.67				
18																	
19	load cell	100		100		100		100		100		100	G1c init: 847.13± 81 N/m G1c prop: 640.90± 46 N/m				
20																	
21																	
22																	

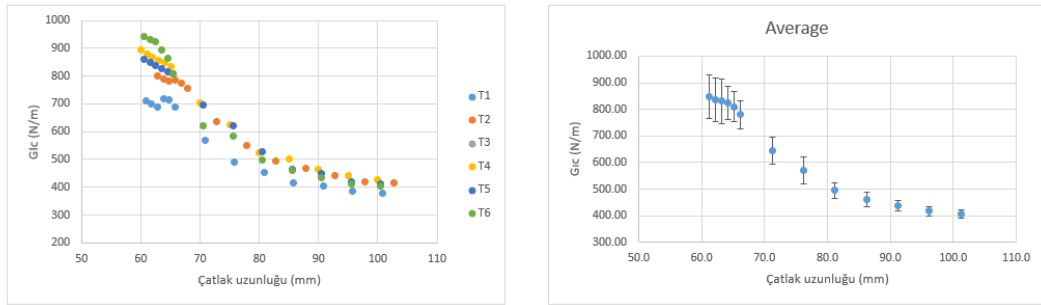


Figure C 8 Plot of G_{1c} versus displacement graph with standard deviation.

Moreover, DCB test machine measured all load, time and displacement data continuously. By using continuous load and displacement data obtained from DCB test machine, load versus displacement graph is plotted for each composite laminate. One of the examples of this plot is shown in Figure C 9.

	U	V	W	X	Y	Z	AA	AB	AC	AD	AE	AF	AG	AH	AI	AJ	AK	AL	AM	AN	
1	T5					T6					Average										
2	Load (kN)	Displacement (sec)	Load (N)			Load (kN)	Displacement (sec)	Load (N)			Load (N)	Displacement (mm)									
3	0	0	0	0		0	0.0001	0	0		0	0.001905									
4	0	0	0.16016	0		0	0.0001	0.16016	0		0	0.001905									
5	0	0.01123	0.40234	0		0	0.01113	0.39063	0		0	0.010623333									
6	0	0.01123	0.61719	0		0	0.01113	0.61719	0		0	0.010623333									
7	0	0.01872	0.84375	0		0	0.01862	0.84375	0		0	0.016831667									
8	0	0.01872	1.07422	0		0	0.01862	1.07422	0		0	0.018113333									
9	0	0.02621	1.30078	0		0	0.0257	1.30078	0		0	0.023003333									
10	0	0.03329	1.59766	0		0	0.03269	1.57422	0		0	0.030125									
11	0	0.03329	1.75781	0		0	0.03269	1.75781	0		0	0.031373333									
12	0	0.04028	1.99219	0		0	0.04018	1.98828	0		0	0.037495									
13	0	0.04028	2.21484	0		0	0.04018	2.21484	0		0	0.03876									
14	0	0.04787	2.44531	0		0	0.04726	2.44141	0		0	0.044833333									
15	0	0.04787	2.67188	0		0	0.04726	2.67188	0		0	0.046046667									
16	0	0.05536	2.90234	0		0	0.05485	2.89844	0		0	0.053485									
17	0	0.06244	3.19141	0		0	0.06234	3.18359	0		0	0.059658333									
18	0	0.06244	3.35547	0		0	0.06234	3.35547	0		0	0.06089									
19	0	0.06993	3.60156	0		0	0.06983	3.58984	0		0.16667	0.06708									
20	0	0.06993	3.8125	0		0	0.06983	3.8125	0		0.33333	0.068293333									
21	0	0.07752	4.04297	0		0	0.07711	4.04297	0		0.33333	0.075611667									
22	0	0.07752	4.26953	0		0	0.07711	4.26953	0		0.33333	0.07804									
23	0	0.0846	4.5	0		0	0.0845	4.5	0		0.33333	0.082931667									
24	0	0.09199	4.80078	0		0	0.09209	4.80469	0		0.33333	0.090353333									
25	0	0.09199	4.95703	0		0.001	0.09209	4.95703	1		0.5	0.090353333									

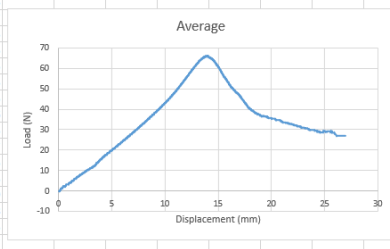


Figure C 9 Plotting graph by using load and displacement data which are measured continuously during the test.